Proposal of pseudo-intrinsic dynamic nature of interactions: simple methods to generate the perturbed structures and to analyze for the prediction of the nature of high reliability, with the applications

Satoko Hayashi,* Taro Nishide, Hikaru Matsuoka, Ryosuke Imanaka, and Waro Nakanishi*

Faculty of Systems Engineering, Wakayama University, 930 Sakaedani, Wakayama 640-8510, Japan
Email: hayashi3@sys.wakayama-u.ac.jp and nakanisi@sys.wakayama-u.ac.jp

Dedicated to Professor Józef Drabowicz on the occasion of his 75th birthday

Abstract

Highly reliable dynamic nature of interactions is obtained with QTAIM dual functional analysis, if the perturbed structures generated by CIV, the established method, are used. Simpler and easier methods are proposed to predict the nature, with the same reliability as that with CIV. The dynamic nature using the structures generated with the partial optimization method is described as the ''pseudo intrinsic dynamic nature of interactions,'' since it satisfies the requirements. An ultimate method, called OMA, is proposed to generate them. Two perturbed structures are shown to be enough, instead of four. The proposed methods were applied to some noncovalent interactions.
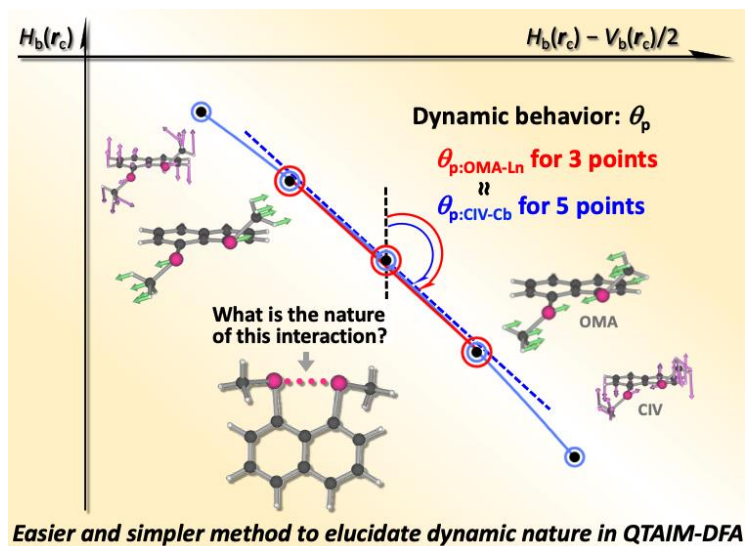
Easier and simpler method to elucidate dynamic nature in QTAIM-DFA

Introduction

Weak interactions determine the fine details of structures and create high functionalities to materials, while strong bonds form the molecular skeletons. Therefore, they are of current and continuous interest.[1–16] It is a most important issue to control the weak interactions, experimentally and theoretically, in chemical and biological sciences. It is the first stage of investigations to clarify the nature of the chemical bonds and interactions. In our investigation, the nature of an interaction in question will not be defined based on the interaction in formal structural features but is determined by considering the character of the interaction. Namely, the nature of an interaction is predicted to have vdW nature, if the interaction shows the typical character of the vdW interaction, for instance. In this process, it is necessary to define the scope of the typical character of each interaction, which should arise from the typical electronic structure of the interaction.

How can the scope of the nature of interactions be defined? The chemical bonds and interactions are classified using the quantum theory of atoms-in-molecules (QTAIM) approach, introduced by Bader.[17,18] However, it seems difficult to characterize the noncovalent interactions with QTAIM. Thus we proposed QTAIM dual functional analysis (QTAIM-DFA), after the QTAIM approach.[19–24] QTAIM-DFA incorporates the QTAIM approach. QTAIM-DFA has excellent potential to classify, characterize, and understand weak to strong interactions, according to a unified form.[20–24] However, the full treatment of QTAIM-DFA has some difficulties, especially for experimental chemists who are not familiar with such treatments. The purpose of this paper is to propose simpler and easier methods for QTAIM-DFA, of the substantially same reliability as the full treatment.

QTAIM-DFA and QTAIM approaches are explained first, followed by the suggestions to promote research in this work.

Survey of QTAIM-DFA and QTAIM approach

A chemical bond or an interaction between A and B is denoted by A−B, which corresponds to the bond path (BP) in QTAIM. We use A-∗-B for the BP, where the asterisk emphasizes the existence of a bond critical point[17,18,25] (BCP; ∗) in A−B.[19–24] BCP is a point along the interatomic bond path at the interatomic surface where the charge density $\rho(r)$ reaches a minimum, while its maximum is on the interatomic surface separating the atomic basins. The $\rho(r)$ values at BCPs are described by $\rho_b(r_c)$, so are other QTAIM functions at BCPs, such as the total electron energy densities $H_b(r_c)$, potential energy densities $V_b(r_c)$, and kinetic energy densities $G_b(r_c)$. Eqs. (1), (2), and (2') show the relations among the functions (*cf*: Virial theorem for eq. (2)).

$$H_b(r_c) = G_b(r_c) + V_b(r_c) \tag{1}$$
$$(\hbar^2/8m)\nabla^2\rho_b(r_c) = H_b(r_c) - V_b(r_c)/2 \tag{2}$$
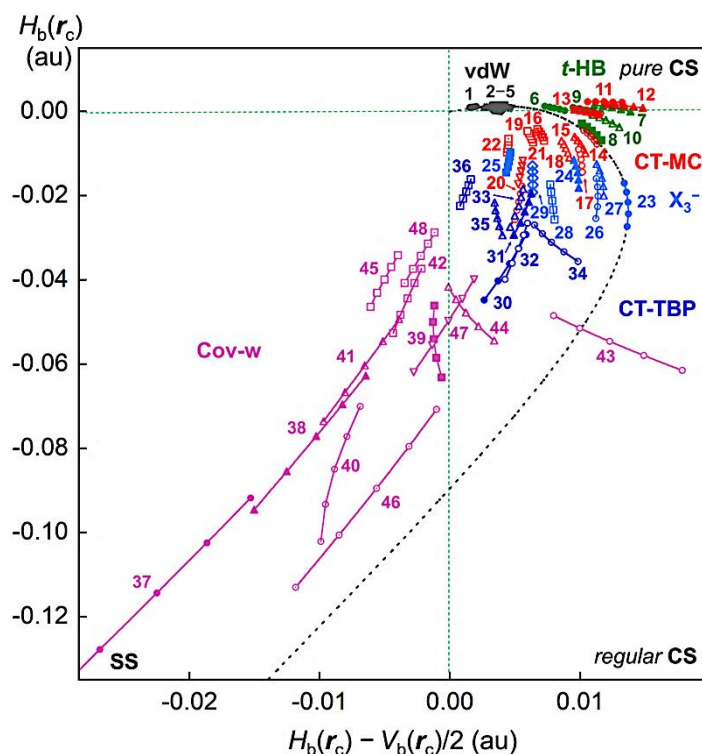$$= G_b(r_c) + V_b(r_c)/2 \tag{2'}$$

Chemical bonds and interactions are classified by the signs of $\nabla^2\rho_b(r_c)$ and $H_b(r_c)$. They are called shard shell (SS) interactions when $\nabla^2\rho_b(r_c) < 0$ and closed-shell (CS) interactions when $\nabla^2\rho_b(r_c) > 0$.[20–24] In particular, the CS interactions are called *pure* CS (*p*-CS) interactions when $H_b(r_c) > 0$ and $\nabla^2\rho_b(r_c) > 0$. We propose to call the interactions of $H_b(r_c) < 0$ and $\nabla^2\rho_b(r_c) > 0$ *regular* CS (*r*-CS) interactions, which distinguish clearly these interactions from the *p*-CS interactions. The signs of $\nabla^2\rho_b(r_c)$ can be replaced by those of $H_b(r_c) - V_b(r_c)/2$ because $(\hbar^2/8m)\nabla^2\rho_b(r_c) = H_b(r_c) - V_b(r_c)/2$ (see eq. (2)). While $H_b(r_c) - V_b(r_c)/2 = 0$ corresponds to the borderline between the classic covalent bonds (Cov) of SS and the noncovalent interactions of CS, $H_b(r_c) = 0$ appear to be buried in the CS interactions. Consequently, it is difficult to characterize the CS interactions of

van der Waals (vdW) type, typical hydrogen bonds (*t*-HBs) with no covalency (*t*-HB$_{nc}$), *t*-HBs with covalency (*t*-HB$_{wc}$), molecular complexes formed through charge transfer (CT-MCs), trihalide ions (X$_3^-$), and trigonal bipyramidal adducts formed through CT (CT-TBPs), if analyzed based on the signs of $H_b(r_c) - V_b(r_c)/2$ and/or $H_b(r_c)$. Cov is sub-divided into Cov-s (Cov strong) and Cov-w (Cov weak), when $R > 0.15$ au and $R < 0.15$ au, respectively, as shown in Table 1, where the definition of R will be explained later.

In QTAIM-DFA, $H_b(r_c)$ are plotted versus $H_b(r_c) - V_b(r_c)/2$ [$(\hbar^2/8m)\nabla^2\rho_b(r_c)$] at BCPs, instead of $H_b(r_c)$ versus $\nabla^2\rho_b(r_c)$. This choice enables us to analyze the plots much morre effectively, since the four arithmetic operations can be applied to analyze the plots by unifying the unit of both axes in the plot to energy. Figure 1 shows the QTAIM-DFA plots of $H_b(r_c)$ versus $H_b(r_c) - V_b(r_c)/2$ for various noncovalent and some weak covalent interactions. (See Table 3 for the data plotted in Figure 1, calculated under MP2/S-TZPsp, where the perturbed structures are generated with the partial optimization method of the Modredundant form (POM-M).)

The plots in Figure 1 have a spiral stream as a whole and the interactions seem well separated. The interactions are expected to be well classified and characterized with QTAIM-DFA.

Recently, calculations of species containing atoms of the 5th period have been carried out more and more. We must be careful when the dynamic nature of **34**, **35**, **39**, **40**, **43**, **44**, and **51** are discussed, since the plots show an irregular stream, compared with others. The Te and I atoms of the 5th period are contained in **34**, **35**, **39**, **43**, **44**, and **51**, while **40** contains Se-∗-Cl. (Details will be discussed elsewhere.)

Figure 1. QTAIM-DFA plots of $H_b(r_c)$ versus $H_b(r_c) - V_b(r_c)/2$ for **1–48** of vdW, HB, CT-MC, X$_3^-$, CT-TBP of CS, and some Cov-w of SS, where the perturbed structures are generated employing POM-M, under MP2/S-TZPsp. The numbers and colors in the figure are the same as those in Table 3.

In our treatment, data from the perturbed structures around the fully optimized structures are employed, in addition to those that are fully optimized. Data from the fully optimized structures are analyzed using the polar coordinate (R, θ) representation, which corresponds to the static nature of interactions.[20–24] Each interaction plot, containing data from both perturbed and fully optimized structures, is expressed by (θ_p, κ_p),

where θ_p corresponds to the tangent line of the plot and κ_p is the curvature. θ and θ_p are measured from the *y*-axis and the *y*-direction, respectively. The concept of the dynamic nature of interactions has been proposed based on (θ_p, κ_p).[20–24] (See Figures 1 and 2, footnotes of Tables 3 and 4, and the Appendix of Supporting Information for the definitions of the QTAIM-DFA parameters of (R, θ) and (θ_p, κ_p)). As a result, the signs of d($H_b(r_c)$ − $V_b(r_c)/2$)/d*r* and d$H_b(r_c)$/d*r*, where *r* is the interaction distance, are employed to characterize interactions in QTAIM-DFA, while the signs of $H_b(r_c)$ − $V_b(r_c)/2$ and $H_b(r_c)$ are used to classify them, overall. Namely, θ classifies interactions, while θ_p characterizes them.

The reliability of the dynamic nature is controlled by the quality of the perturbed structures. We have proposed three methods to generate the perturbed structures for QTAIM-DFA, so far. They are called POM,[20,21] NIV,[22,23] and CIV.[26] The perturbed structures are generated by the partial optimizations in POM with the interaction distances in question being fixed appropriately longer and shorter than the fully optimized distances (according to eq. (3)). POM is the thermal process. POM of the Z-matrix form, called POM-Z, was used in the early stage of the investigations. The reliability of the dynamic nature will be examined carefully in this work, when the perturbed structures are generated with POM of the Modredundant form (POM-M). The normal coordinates of the (best-fitted) internal vibrations are used to generate the perturbed structures in NIV. The perturbed structures with NIV are the mathematical similarity to those appearing in the zero-point internal vibrations. NIV is the adiabatic process.

In CIV, the coordinates derived from the compliance constants C_{ii} for the internal vibrations are employed to generate the perturbed structures, instead of the normal coordinates in NIV. The compliance constants C_{ij} are defined as the partial second derivatives of the potential energy due to an external force, as shown in eq. (R1).[26,27] CIV corresponds to an improved method of NIV, therefore, it should be recognized as an adiabatic process. CIV is demonstrated to be the highly reliable method to generate the perturbed structures for QTAIM-DFA.[20–24] QTAIM-DFA with CIV has excellent potential to classify, characterize, and understand weak to strong interactions with high reliability, according to a unified form. The dynamic nature of interactions with CIV is described as the "intrinsic dynamic nature of interactions," since the coordinates in CIV are invariant to the choice of coordinate system.

QTAIM-DFA with CIV were applied to the standard interactions consisting of the atoms of the 1st–4th periods. The rough criteria that distinguish the interaction in question from others were obtained, at the early stage of the investigations, under MP2/6-311++G(3df,3pd). QTAIM-DFA and the criteria are explained in the Appendix of the Supporting Information, using Schemes SA1–SA3, Figs. SA1 and SA2, Table SA1, and eqs. (SA1)–(SA7).

Figure 2 summarizes the areas for the standard interactions of vdW type, t-HB$_{nc}$, t-HB$_{wc}$, CT-MCs, X$_3^−$, and CT-TBPs, together with Cov-w and Cov-s, which appear in the QTAIM-DFA plot of $H_b(r_c)$ versus $H_b(r_c)$ − $V_b(r_c)/2$. The areas seem defined uniquely for most interactions by the QTAIM-DFA parameters, while the areas are determined tentatively for some interactions, so as to be accepted by experimental scientists. Table 1 summarizes the criteria, derived from the areas illustrated in Figure 2, which are the most basic results in QTAIM-DFA. The (θ, θ_p) values of (75°, **90°**), (**90°**, 125°), (115°, 150°), (150°, **180°**) and (**180°**, 190°) correspond to the borderlines between the vdW/t-HB$_{nc}$, t-HB$_{nc}$/t-HB$_{wc}$, t-HB$_{wc}$/CT-MC, CT-MC/CT-TBP and CT-TBP/Cov interactions, respectively (see Table 1). The basic values of (θ, θ_p), described in bold, are superior to the tentatively given values (in plane) in the classification and characterization of interactions. The θ values of 45.0° < θ < 90.0°, 90.0° < θ < 180.0°, and 180.0° < θ < 206.6° correspond to the *p*-CS, *r*-CS, and SS interactions, respectively.
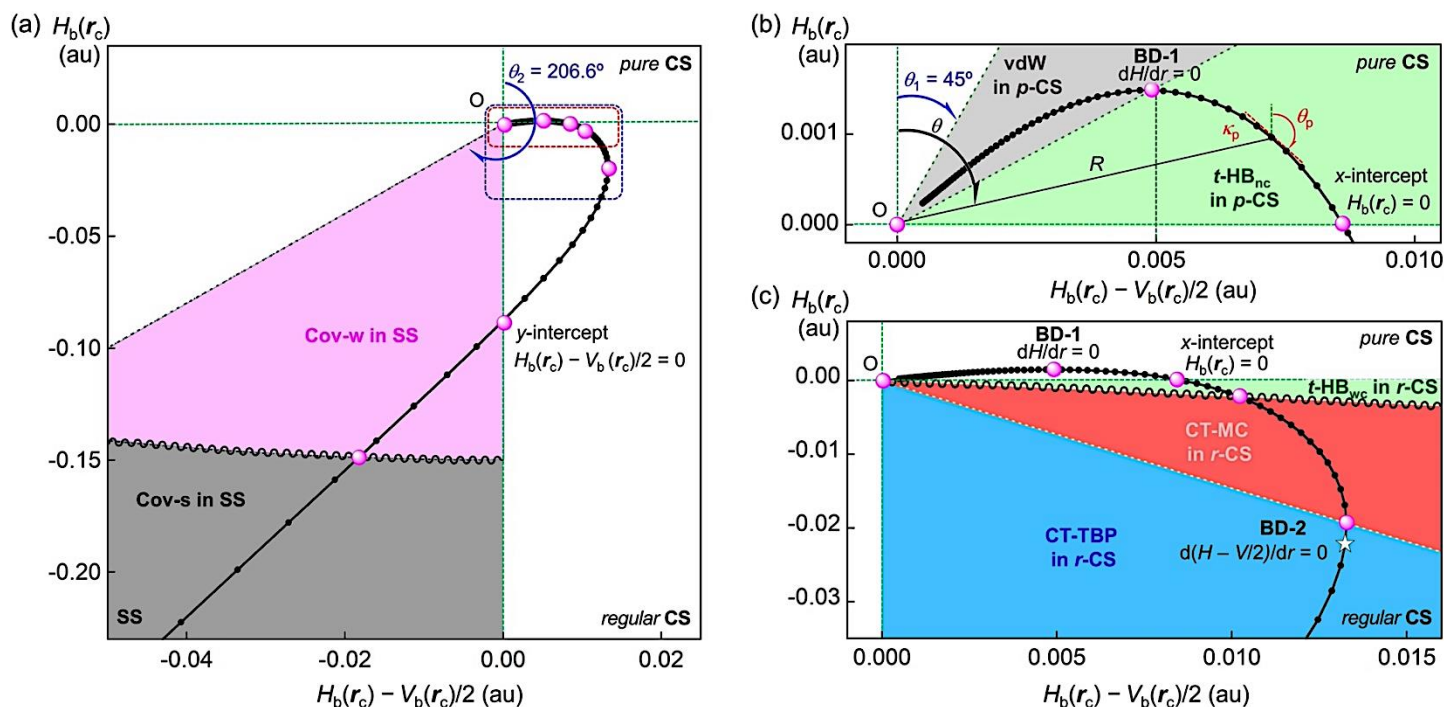
Figure 2. Areas for the weak to strong interactions which appear in the plot of $H_b(r_c)$ versus $H_b(r_c) - V_b(r_c)/2$, calculated under MP2/6-311++G(3df,3pd). Data for Cl-Cl-*-Cl⁻ over a wide range of w in eq. (3) being employed for the plot. (a) Whole picture, (b) magnified one for the *p*-CS region, and (c) magnified one for the *r*-CS region. The white asterisk in (c) corresponds to the optimized structure. The θ_1 (= 45°) and θ_2 (= 206.6°) values correspond to the limited values. The definitions of (R, θ) and (θ_p, κ_p) are illustrated (b). First and second bending points of the plot (BD-1 and BD-2, respectively) are also shown.

Table 1. Ranges of (R, θ, θ_p), required to predict the nature of the interactions, based on the criteria formulated under MP2/6-311++G(3df,3pd)

Natures	Requirement[a]		
p-CS/vdW	45° < θ < 75°;	45° < θ_p < **90°**	
p-CS/*t*-HB$_{nc}$	75° < θ < **90°**;	**90°** < θ_p < 125°	
r-CS/*t*-HB$_{wc}$	**90°** < θ < 115°;	125° < θ_p < 150°	
r-CS/CT-MC	115° < θ < 150°;	150° < θ_p < **180°**	
r-CS/CT-TBP+X$_3^-$	150° < θ < **180°**;	**180°** < θ_p < 190°	
SS/Cov-w	**180°** < θ < 206.6°;	190° < θ_p < 206.6°;	R < 0.15 au
SS/Cov-s	**180°** < θ < 206.6°;	190° < θ_p < 206.6°;	R > 0.15 au

[a] The basic parameters, described in bold, are superior to the tentatively given parameters, described in plain, in the prediction of interactions.

Guides to the new methodologies

QTAIM-DFA with CIV is the excellent method to predict the dynamic and static natures of interactions. However, it is necessary to handle the complex compliance program in the process with CIV, which would be difficult for those not familiar with the theoretical treatment. Therefore, we searched for simpler and easier methodologies to generate the perturbed structures of very high quality, other than CIV.

How can new simpler and easier methods be devised? We have recognized that the perturbed structures generated with POM-Z have the quality very close to that with CIV, since CIV has been proposed.[26] Using this as a clue, substantial effort was paid to inflate the image for the establishment of the simpler and easier methods to analyze the interactions effectively. Figure 3 shows the plot of $H_b(r_c)$ versus $H_b(r_c) - V_b(r_c)/2$ for the data of the fully optimized structures, exemplified by Cl-Cl-∗-Cl⁻, together with those from the perturbed structures generated with CIV, POM-Z, POM-M, and NIV of the symmetric and anti-symmetric vibrations (abbreviated by NIV$_s$ and NIV$_{as}$, respectively). The perturbed structures were also used to generate by changing only the interaction distance in question (called the major interaction) in Cl-Cl-∗-Cl⁻. The method is called OMA. Figure 3 contains the plot with OMA. The plots are analyzed using the QTAIM-DFA parameters of (R, θ) and (θ_p, κ_p), as explained above. The θ_p values based on the methods to generate the perturbed structures are given in Tables 3 and 4. The reliability of the dynamic nature of the interaction can be recognized based on the θ_p values.
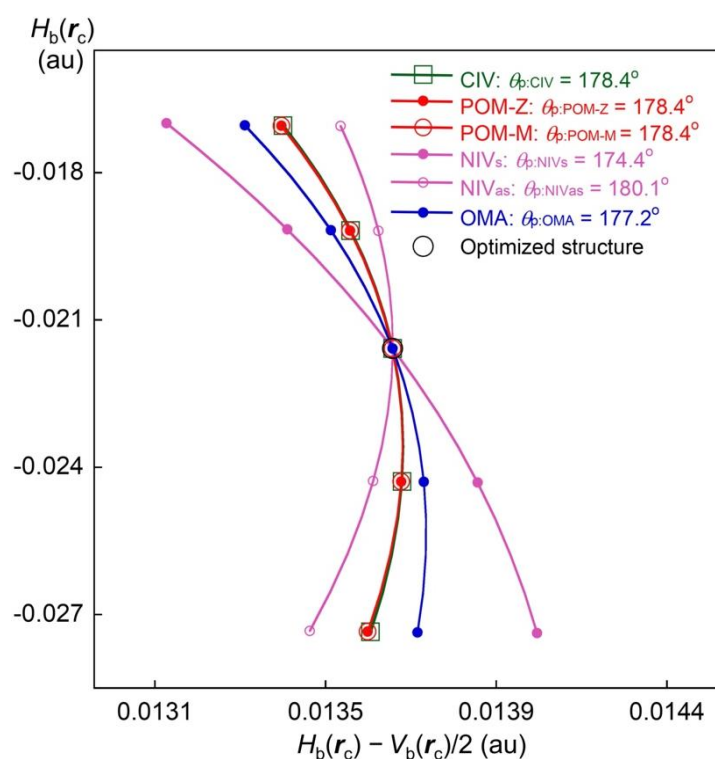
Figure 3. QTAIM-DFA plots of $H_b(r_c)$ versus $H_b(r_c) - V_b(r_c)/2$ for [Cl-Cl-∗-Cl]⁻ ($D_{\infty h}$), where the perturbed structures are generated with CIV, POM-Z, POM-M, NIV$_s$, NIV$_{as}$, and OMA. The θ_p values are given in the figure.

As shown in Figure 3 (and Table 3 and Table S3 of the Supporting Information), the θ_p values are 178.4° for the three methods of CIV, POM-Z, and POM-M. The θ_p values with NIV$_s$ and NIV$_{as}$ are 174.4° and 180.1°, respectively. The θ_p value is 177.2° with OMA. It is demonstrated that the quality of the perturbed structures generated with POM-Z and POM-M is the same as that with CIV.[26] The θ_p values with NIV$_s$ and NIV$_{as}$ are smaller and larger than that with CIV by 4.0° and 1.7°, respectively. The θ_p value with OMA is smaller than that with CIV by 1.2°. The results show that OMA is better than NIV to generate the perturbed structures, since the magnitudes in the differences from CIV is smaller for OMA than the case of NIV$_s$ and NIV$_{as}$. Indeed, POM-Z and POM-M can be recognized as the same methods as CIV, but POM-M seems superior to POM-Z, since POM-Z has some disadvantages in constructing the perturbed structures and in the optimizations,[28] especially when it is applied to large and/or complex species. POM-M would release such disadvantages in POM-Z. OMA will

show good advantages, when applied to large and/or complex molecules, although some devices would be necessary. We will mainly examine POM-M and OMA, here, as the simpler and easier methods to generate the perturbed structures for QTAIM-DFA.

Four perturbed structures and a fully optimized one, with the regression curve of a cubic function, are necessary to predict the dynamic nature for an interaction, in the full treatment of QTAIM-DFA. Two perturbed structures and a fully optimized one, with a regression curve of a linear type, also give the dynamic nature for the interaction. If the predicted dynamic nature based on the latter is demonstrated to be substantially the same as that based on the former, the latter method can be recognized as the simpler and easier methodology. The reliability was also examined by comparing the two results. Indeed, the κ_p values cannot be obtained with a linear regression curve, but it does not damage our discussion, since κ_p is not used in the prediction of the natures.

Here, we present the results of the investigations, searching for the simpler and easier methods for QTAIM-DFA. The dynamic nature with POM (POM-Z and POM-M) we propose to term "pseudo intrinsic dynamic nature of interactions," after the establishment of the same reliability of the dynamic nature with POM as that with CIV. POM-M seems superior to POM-Z, as the simpler and easier method. The reliability of the dynamic nature obtained using two perturbed structures and a fully optimized one, with a regression curve of a linear type, is substantially the same as that in the full treatment. The reliability with OMA also seems substantially high, which should be the ultimate simpler and easier method to generate the perturbed structures. The applied results of the proposed methods are also discussed.

The purpose of this paper is to present a simpler and easier method for experimental chemists to be able to predict the nature of interactions in question with high reliability. We believe that by applying the proposed methods, experimental chemists will be released from concerns about the complex compliance program and from the frequency analysis in the prediction of the dynamic nature of interactions with QTAIM-DFA.

Methodological Details in Calculations

General. Calculations were performed employing the Gaussian 09 programs package.[29] Structures of the selected species **1–56** were optimized, where **1–4**, **6–12**, **14**, **15**, **17**, **18**, **23**, **24**, **26**, **27**, **30–33**, **37**, **38**, **40**, **41**, **46**, **47**, **49**, **50**, and **52–56** consist of the atoms in the 1st–4th periods, while **1–56** other than above contain Te, I, and Xe atoms in the 5th period (see Table 1).[30] The Sapporo-TZP basis set with 1s1p diffusion functions (abbreviated by S-TZPsp), as implemented from Sapporo Basis Set Factory,[31,32] was applied to all atoms in **1–56**. Calculations were performed at the Møller-Plesset second-order energy correlation (MP2) level (MP2/S-TZPsp). The optimized structures were confirmed by frequency analysis. The tight optimization mode was applied to all species and the very tight mode, if necessary. The results of the frequency analysis were used to obtain the C_{ij} values and the coordinates corresponding to C_{ii} ($\mathbf{C}_i$). It is necessary to use such a calculation method that reproduces well the observed structures, if the nature of the interactions are to be determined on the observed structures or very close to them.[33] The MP2/S-TZPsp method will afford reliable results in the calculations of the systems, containing the atoms of the 5th period.

In POM, the fully optimized structures are further (partially) optimized with r being fixed to satisfy eq. (3), where r and r_o are the interaction distances in question in the perturbed and fully optimized structures, respectively, and a_o is the Bohr radius (0.52918 Å).[20,21] The optimized values of r' (i.e., other than r) are described by eq. (4). We call r and r' the major and minor interactions, respectively.[34] Eqn (5) explains the method to generate the perturbed structures with CIV. An i-th perturbed structure in question ($\mathbf{S}_{iw}$) is

generated by the addition of the coordinates (C_i), derived from C_{ii}, to the standard orientation of a fully optimized structure (S_o) in the matrix representation.[26] The coefficient g_{iw} in eq. (5) controls the structural difference between S_{iw} and S_o: g_{iw} is determined to satisfy eq. (3) for the interaction in question. The C_i values of six digits are used to predict S_{iw}. Data were analyzed with the AIM2000[35] and AIMAll[36] programs.

$$r = r_o + wa_o \ (w = (0), \pm 0.05, \text{ and } \pm 0.1; a_o = 0.52918 \text{ Å}) \tag{3}$$

$$r' = r_o' + w'a_o \tag{4}$$

$$S_{iw} = S_o + g_{iw} \bullet C_i \tag{5}$$

$$y = c_o + c_1 x + c_2 x^2 + c_3 x^3 \tag{6}$$

$$y = c_o' + c_1' x \tag{7}$$

In the full treatment of QTAIM-DFA, $H_b(r_c)$ are plotted versus $H_b(r_c) - V_b(r_c)/2$ for the data of five points (w = 0, ±0.05, and ±0.1 in eq. (3)). Eq. (6) is applied when each plot is analyzed using a regression curve of the cubic function in this process (R_c^2 (square of correlation coefficient) > 0.99999 usually). Data of three points (w = 0 and ±0.05 in eq. (3)) are used in the simpler method. The regression curve of the linear function (eq. (7)) is similarly applied for the analysis. Only θ_p can be obtained in this process.

Results and Discussion

High similarities between the perturbed structures generated with POM-M, POM-Z and CIV

The structures of the selected species (**1–56**) were optimized with MP2/S-TZPsp. The interaction distances in question for **1–56** calculated with MP2/S-TZPsp are collected in Table S1 of the Supporting Information. The perturbed structures at w = ±0.05 and ±0.1 in eq. (3) were generated with POM-M, POM-Z and CIV. The w' values for the most important minor interactions in the perturbed structures are calculated at w = 0.1 of the major interactions, according to eq. (4). The w'/w ratios should be the reflection from the effects of the major interactions on the minor ones and closely related to the perturbed structures, as pointed out before.[28] The ratios are calculated in the perturbed structures generated with POM-M ((w'/w)POM-M), POM-Z ((w'/w)POM-Z), and CIV ((w'/w)CIV). The (w'/w)POM-M, (w'/w)POM-Z, and (w'/w)CIV values are collected in Table S2 of the Supporting Information. The (w'/w)POM-M, (w'/w)POM-Z, and (w'/w)CIV values are less than approximately 0.4, which shows that the magnitudes of the displacements of the minor interactions are less than about 0.4 times larger than those of the fixed major ones. The (w'/w)POM-M and (w'/w)POM-Z values are plotted versus (w'/w)CIV. The plots are shown in Figure S1 of the Supporting Information. The plots are analyzed assuming the linear correlations of $y = ax + b$ (a: correlation constant, b: y-intercept, and R_c^2: the square of the correlation coefficient). The plots gave excellent correlations. The (w'/w)POM-M values are also plotted versus (w'/w)POM-Z, although not shown in a figure. The plot also gives an excellent correlation. Table 2 collects the correlations (entries 1–3, respectively). The perturbed structures generated with POM-M, POM-Z, and CIV under MP2/S-TZPsp are shown to be very close with each other for **1–56**. The results are the firm basis for the starting point of this investigation.

Table 2. Correlations between the parameters, evaluated using the perturbed structures generated with POM-M, POM-Z, and CIV under MP2/S-TZPsp

Entry	Correlation	Method	a	b	R_c^2	Correlation with n
1	$w'/w_{:POM-M}$ vs $w'/w_{:CIV}$	MP2/S-TZPsp	0.968	-0.0005	0.9987	52^a (Fig. S1)
2	$w'/w_{:POM-Z}$ vs $w'/w_{:CIV}$	MP2/S-TZPsp	0.967	-0.0005	0.9986	52^a (Fig. S1)
3	$w'/w_{:POM-M}$ vs $w'/w_{:POM-Z}$	MP2/S-TZPsp	1.0008	-0.00003	0.99992	52^a
4	$\theta_{p:POM-M}$ vs $\theta_{p:CIV}$	MP2/S-TZPsp	1.0003	-0.038	0.99999	56 (Fig. 4)
5	$\theta_{p:POM-Z}$ vs $\theta_{p:CIV}$	MP2/S-TZPsp	0.9998	0.021	0.99999	56 (Fig. 4)
6	$\theta_{p:POM-M}$ vs $\theta_{p:POM-Z}$	MP2/S-TZPsp	1.0006	-0.058	0.99998	56
7	$\kappa_{p:POM-M}$ vs $\kappa_{p:CIV}$	MP2/S-TZPsp	1.0001	0.73	0.9977	56 (Fig. 5)
8	$\kappa_{p:POM-Z}$ vs $\kappa_{p:CIV}$	MP2/S-TZPsp	0.9995	0.71	0.9982	56 (Fig. 5)
9	$\kappa_{p:POM-M}$ vs $\kappa_{p:\ POM-Z}$	MP2/S-TZPsp	1.0006	0.02	0.9995	56
10	$\theta_{p:POM-M-Ln}$ vs $\theta_{p:POM-M-Cb}$	MP2/S-TZPsp	0.9992	0.16	0.99999_4	56 (Fig. 6)
11	$\theta_{p:OMA-Ln}$ vs $\theta_{p:POM-M-Cb}$	MP2/S-TZPsp	0.9972	-0.03	0.9994	56 (Fig. 7)
12	$\theta_{p:OMA-Ln}$ vs $\theta_{p:POM-M-Cb}$	MP2/S-TZPsp	0.9966	0.23	0.9997	53^b (Fig. 7)

[a] Omitting the data from diatomic molecules for **46–48** and **56**. [b] Omitting the data from **10**, **14**, and **17**.

QTAIM functions and QTAIM-DFA parameters calculated with POM-M, POM-Z, and CIV

QTAIM functions are calculated under MP2/S-TZPsp for the interactions in question of **1–56** at the BCPs with POM-M, POM-Z and CIV under MP2/S-TZPsp. The values of $\rho_b(r_c)$, $(\hbar^2/8m)\nabla^2\rho_b(r_c)$ (= $H_b(r_c) - V_b(r_c)/2$), $H_b(r_c)$, $k_b(r_c)$ (= $V_b(r_c)/G_b(r_c)$), and C_{ii} are collected in Table S3 of the Supporting Information. Figure 1 shows the plots of $H_b(r_c)$ versus $H_b(r_c) - V_b(r_c)/2$ for CS of vdW, t-HB$_{nc}$, t-HB$_{wc}$, CT- MC, X$_3^-$, and CT-TBP and SS of Cov-w, where the perturbed structures are generated with POM-M. The plots for Cov-w and Cov-s of SS are similarly drawn in Figure S2 of the Supporting Information.

　　　The QTAIM-DFA parameters of (R, θ) and (θ_p, κ_p) are obtained by analyzing the plots shown in Figure 1 and Figure S2 of the Supporting Information, according to eqs. (SA3)–(SA7) in the Appendix of the Supporting Information. The (θ_p, κ_p) values calculated with POM-M, POM-Z and CIV are denoted by $(\theta_{p:POM-M}, \kappa_{p:POM-M})$, $(\theta_{p:POM-Z}, \kappa_{p:POM-Z})$, and $(\theta_{p:CIV}, \kappa_{p:CIV})$, respectively. Table 3 collects the values, together with the (R, θ) values. The (θ_p, κ_p) values may change depending on the methods to generate the perturbed structures, however, the differences in the parameters calculated with the three methods are negligibly small.

　　　The next step is to establish the high reliability of the dynamic nature for **1–56** with POM-M and POM-Z under MP2/S-TZPsp, after calculating the QTAIM-DFA parameters with POM-M, POM-Z, and CIV under MP2/S-TZPsp.

Table 3. QTAIM-DFA Parameters of (R, θ) and (θ_p, κ_p) for the Standard Interactions in **1–56**, Calculated with QTAIM-DFA under MP2/S-TZPsp, Employing the Perturbed Structures Generated with POM-M, POM-Z, and CIV[a]

Species (X-*-Y) (No: symmetry)	R^b (au)	θ^c (°)	$\theta_{p:POM-M}^d$ (°)	$\kappa_{p:POM-M}^e$ (au^{-1})	$\theta_{p:POM-Z}^d$ (°)	$\kappa_{p:POM-Z}^e$ (au^{-1})	$\theta_{p:CIV}^d$ (°)	$\kappa_{p:CIV}^e$ (au^{-1})	Predicted nature
He-*-HF (**1**: $C_{\infty v}$)	0.0020	58.9	62.3	69.8	62.3	69.8	62.3	69.8	*p*-CS/vdW
Ne-*-HF (**2**: $C_{\infty v}$)	0.0032	70.3	77.8	16.0	77.8	16.0	77.8	16.0	*p*-CS/vdW
Ar-*-HF (**3**: $C_{\infty v}$)	0.0040	69.1	83.4	157.2	83.4	157.2	83.4	157.2	*p*-CS/vdW
Kr-*-HF (**4**: $C_{\infty v}$)	0.0044	78.9	106.2	211.9	106.2	211.9	106.2	211.4	*p*-CS/*t*-HB$_{nc}$
Xe-*-HF (**5**: $C_{\infty v}$)	0.0037	81.3	109.9	278.8	109.9	278.8	109.9	277.8	*p*-CS/*t*-HB$_{nc}$
NN-*-HF (**6**: $C_{\infty v}$)	0.0081	84.2	123.3	157.9	123.3	158.0	123.3	156.9	*p*-CS/*t*-HB$_{nc}$
HF-*-HF (**7**: C_s)	0.0125	85.8	117.9	124.5	117.9	124.1	117.9	125.2	*p*-CS/*t*-HB$_{nc}$
HCN-*-HF (**8**: $C_{\infty v}$)	0.0118	113.0	159.1	51.2	159.1	51.2	159.0	49.1	*r*-CS/CT-MC
H$_2$O-*-HOH (**9**: C_s)	0.0105	88.0	123.4	129.1	123.5	130.2	123.4	128.5	*p*-CS/*t*-HB$_{nc}$
Me$_2$O-*-HOH (**10**: C_s)	0.0122	99.8	145.3	78.9	145.3	77.4	145.2	89.4	*r*-CS/*t*-HB$_{wc}$
Me$_2$O-*-Cl$_2$ (**11**: C_s)	0.0121	79.1	93.2	53.2	93.2	52.9	93.2	52.6	*p*-CS/*t*-HB$_{nc}$
Me$_2$O-*-Br$_2$ (**12**: C_s)	0.0135	84.3	107.2	86.5	107.1	86.3	107.2	85.5	*p*-CS/*t*-HB$_{nc}$
Me$_2$O-*-I$_2$ (**13**: C_s)	0.0105	90.3	122.4	123.2	122.5	124.1	122.6	121.9	*r*-CS/*t*-HB$_{wc}$
Me$_2$S-*-Cl$_2$ (**14**: C_s)	0.0124	118.8	162.8	61.5	162.9	56.5	162.9	49.5	*r*-CS/CT-MC
Me$_2$S-*-Br$_2$ (**15**: C_s)	0.0127	127.8	167.4	42.9	167.4	40.1	167.4	38.2	*r*-CS/CT-MC
Me$_2$S-*-I$_2$ (**16**: C_s)	0.0089	128.0	169.1	43.9	169.1	47.5	169.1	42.5	*r*-CS/CT-MC
Me$_2$Se-*-Cl$_2$ (**17**: C_s)	0.0152	138.6	176.9	18.8	176.9	18.8	176.9	18.7	*r*-CS/CT-MC
Me$_2$Se-*-Br$_2$ (**18**: C_s)	0.0125	134.5	170.9	33.7	171.2	36.0	171.0	32.2	*r*-CS/CT-MC
Me$_2$Se-*-I$_2$ (**19**: C_s)	0.0086	133.7	171.3	49.9	170.9	47.8	170.9	41.0	*r*-CS/CT-MC
Me$_2$Te-*-Cl$_2$ (**20**: C_s)	0.0221	166.2	184.3	0.0	183.9	0.1	183.9	0.5	*r*-CS/CT-TBP
Me$_2$Te-*-Br$_2$ (**21**: C_s)	0.0153	159.0	183.7	8.8	183.7	11.3	183.7	9.1	*r*-CS/CT-TBP
Me$_2$Te-*-I$_2$ (**22**: C_s)	0.0092	150.8	182.2	24.9	181.5	21.2	182.0	20.4	*r*-CS/CT-TBP
[Cl-*-Cl$_2$]$^-$ (**23**: $D_{\infty h}$)	0.0255	147.6	178.4	15.0	178.4	15.0	178.4	14.6	*r*-CS/CT-MC
[Br-*-Br$_2$]$^-$ (**24**: $D_{\infty h}$)	0.0175	145.9	176.5	22.9	176.5	22.9	176.5	22.2	*r*-CS/CT-MC
[I-*-I$_2$]$^-$ (**25**: $D_{\infty h}$)	0.0128	159.1	183.8	14.7	183.8	14.7	183.8	14.0	*r*-CS/CT-TBP
[Cl-*-BrCl]$^-$ (**26**: $D_{\infty h}$)	0.0231	150.5	179.9	12.7	179.9	12.7	179.9	12.2	*r*-CS/CT-MC
[Br-*-ClBr]$^-$ (**27**: $D_{\infty h}$)	0.0197	143.6	175.5	23.1	175.5	23.1	175.5	22.7	*r*-CS/CT-MC
[Cl-*-ICl]$^-$ (**28**: $D_{\infty h}$)	0.0226	159.7	177.9	1.0	177.9	1.0	177.9	1.4	*r*-CS/CT-MC
[Br-*-IBr]$^-$ (**29**: $D_{\infty h}$)	0.0171	158.0	180.0	8.3	180.0	8.3	180.0	7.7	*r*-CS/CT-MC
Me$_2$ClS-*-Cl (**30**: C_2)	0.0364	172.8	191.5	6.2	191.5	6.2	191.5	5.4	*r*-CS/CT-TBP
Me$_2$BrS-*-Br (**31**: C_{2v})	0.0245	166.4	187.3	9.7	187.2	8.9	187.4	10.1	*r*-CS/CT-TBP
Me$_2$ClSe-*-Cl (**32**: C_2)	0.0330	170.8	187.4	3.6	187.4	3.6	187.5	3.0	*r*-CS/CT-TBP
Me$_2$BrSe-*-Br (**33**: C_2)	0.0231	166.8	186.0	12.7	186.0	12.7	186.2	8.9	*r*-CS/CT-TBP
Me$_2$ClTe-*-Cl (**34**: C_2)	0.0321	165.9	159.1	28.6	159.1	28.6	159.3	24.7	*r*-CS/CT-MC
Me$_2$BrTe-*-Br (**35**: C_2)	0.0256	171.8	175.7	10.5	175.6	12.2	175.8	12.3	*r*-CS/CT-MC
Me$_2$ITe-*-I (**36**: C_2)	0.0191	176.2	187.5	5.9	187.5	5.9	187.6	1.9	*r*-CS/CT-TBP

(Table 3 continues)

Species (X-*-Y) (No: symmetry)	R^b (au)	θ^c (°)	$\theta_{\text{p:POM-M}}{}^d$ (°)	$\kappa_{\text{p:POM-M}}{}^e$ (au^{-1})	$\theta_{\text{p:POM-Z}}{}^d$ (°)	$\kappa_{\text{p:POM-Z}}{}^e$ (au^{-1})	$\theta_{\text{p:CIV}}{}^d$ (°)	$\kappa_{\text{p:CIV}}{}^e$ (au^{-1})	Predicted nature
Me$_2$S$^+$-*-Cl (**37**: C_s)	0.1165	191.1	197.9	0.3	197.9	0.3	197.9	0.3	SS/Cov-w
Me$_2$S$^+$-*-Br (**38**: C_s)	0.0778	187.6	195.1	0.5	195.1	0.5	195.1	0.5	SS/Cov-w
Me$_2$S$^+$-*-I (**39**: C_s)	0.0542	181.3	178.4	8.3	178.4	8.1	178.4	8.1	SS/Cov-w
Me$_2$Se$^+$-*-Cl (**40**: C_s)	0.0854	185.9	186.0	4.2	186.0	4.4	186.0	4.4	SS/Cov-w
Me$_2$Se$^+$-*-Br (**41**: C_s)	0.0607	186.2	193.5	0.1	193.5	0.1	193.5	0.1	SS/Cov-w
Me$_2$Se$^+$-*-I (**42**: C_s)	0.0445	184.2	188.3	2.2	188.3	2.2	188.3	2.2	SS/Cov-w
Me$_2$Te$^+$-*-Cl (**43**: C_s)	0.0560	167.3	142.7	8.8	142.7	8.8	142.7	8.9	*r*-CS/*t*-HB$_{\text{wc}}$
Me$_2$Te$^+$-*-Br (**44**: C_s)	0.0478	178.5	164.9	14.9	164.9	15.6	164.8	15.6	*r*-CS/CT-MC
Me$_2$Te$^+$-*-I (**45**: C_s)	0.0402	187.2	190.2	2.0	189.6	3.6	189.6	3.6	SS/Cov-w
Cl-*-Cl (**46**: $D_{\infty h}$)	0.0897	183.6	194.3	0.9	194.3	0.9	194.3	0.9	SS/Cov-w
Br-*-Br (**47**: $D_{\infty h}$)	0.0497	180.1	191.8	1.8	191.8	1.8	191.8	1.8	SS/Cov-w
I-*-I (**48**: $D_{\infty h}$)	0.0344	183.7	190.9	0.5	190.9	0.5	190.9	0.5	SS/Cov-w
CH$_3$-*-Cl (**49**: C_{3v})	0.1404	193.9	199.1	0.2	199.1	0.2	199.1	0.2	SS/Cov-w
CH$_3$-*-Br (**50**: C_3)	0.0965	191.9	197.0	0.1	197.0	0.1	197.0	0.1	SS/Cov-w
CH$_3$-*-I (**51**: C_{3v})	0.0694	187.1	179.5	10.4	179.5	10.4	179.5	10.4	SS/Cov-w
CH$_3$-*-CH$_3$ (**52**: D_{3d})	0.2369	199.5	201.8	0.0	201.8	0.0	201.8	0.0	SS/Cov-s
CH$_2$-*-CH$_2$ (**53**: D_{2h})	0.4854	198.3	199.3	0.1	199.3	0.1	199.3	0.1	SS/Cov-s
CH-*-CH (**54**: $D_{\infty h}$)^f	0.6481	194.4	194.4	0.1	194.4	0.1	194.4	0.1	SS/Cov-s
CH$_3$-*-H (**55**: T_d)	0.3718	202.5	201.5	0.4	201.5	0.4	201.5	0.4	SS/Cov-s
H-*-H (**56**: $D_{\infty h}$)	0.4002	206.1	206.4	0.0	206.4	0.0	206.4	0.0	SS/Cov-s

^{a} Data are given for the interaction in question at the BCP, as shown by He-*-HF, for example. ^{b} $R = (x^2 + y^2)^{1/2}$, where $(x, y) = (H_b(r_c) - V_b(r_c)/2, H_b(r_c))$. ^{c} $\theta = 90° - \tan^{-1}(y/x)$. ^{d} $\theta_p = 90° - \tan^{-1}(dy/dx)$. ^{e} $\kappa_p = |d^2y/dx^2| / [1 + (dy/dx)^2]^{3/2}$. ^{f} Data from $w = 0$, ±0.025, and ±0.5 were employed, since the (3, −3) attractor appeared at the center of the perturbed structure for $w = -0.1$.

## High similarities between QTAIM-DFA parameters for 1–56, calculated with POM-M, POM-Z and CIV under MP2/S-TZPsp

Figure 4 shows the plots of $\theta_{\text{p:POM-M}}$ versus $\theta_{\text{p:CIV}}$ and $\theta_{\text{p:POM-Z}}$ versus $\theta_{\text{p:CIV}}$, evaluated under MP2/S-TZPsp. The correlations are excellent, which are collected in Table 2 (entries 4 and 5, respectively). The $\theta_{\text{p:POM-M}}$ values are also plotted versus $\theta_{\text{p:POM-Z}}$, although not shown in a figure. The plot is also excellent, which is given in Table 2 (entry 6). The plots can be substantially recognized as the direct proportion described by $y = x$ ($R_c^2 = 1.00$).

The magnitudes of $\Delta\theta_{\text{p:POM-M–CIV}}$ (= $\theta_{\text{p:POM-M}} - \theta_{\text{p:CIV}}$), $\Delta\theta_{\text{p:POM-Z–CIV}}$ (= $\theta_{\text{p:POM-Z}} - \theta_{\text{p:CIV}}$) and $\Delta\theta_{\text{p:POM-M–Z}}$ (= $\theta_{\text{p:POM-M}} - \theta_{\text{p:POM-Z}}$) are less than or equal to 0.1° for all interactions, except for except for Me$_2$O-*-I$_2$ (**13**: $\Delta\theta_{\text{p:POM-M–CIV}} = -0.2°$), Me$_2$Se-*-Br$_2$ (**18**: $\Delta\theta_{\text{p:POM-Z–CIV}} = 0.2°$; $\Delta\theta_{\text{p:POM-M–Z}} = -0.3°$), Me$_2$Se-*-I$_2$ (**19**: $\Delta\theta_{\text{p:POM-M–CIV}} = 0.4°$; $\Delta\theta_{\text{p:POM-M–Z}} = 0.4°$), Me$_2$Te-*-Cl$_2$ (**20**: $\Delta\theta_{\text{p:POM-M–CIV}} = 0.4°$; $\Delta\theta_{\text{p:POM-M–Z}} = 0.4°$), Me$_2$Te-*-I$_2$ (**22**: $\Delta\theta_{\text{p:POM-M–CIV}} = 0.2°$; $\Delta\theta_{\text{p:POM-Z–CIV}} = -0.5°$; $\Delta\theta_{\text{p:POM-M–Z}} = 0.7°$), Me$_2$BrS-*-Br (**31**: $\Delta\theta_{\text{p:POM-Z–CIV}} = -0.2°$), Me$_2$BrSe-*-Br (**33**: $\Delta\theta_{\text{p:POM-M–CIV}} = -0.2°$; $\Delta\theta_{\text{p:POM-Z–CIV}} = -0.2°$), Me$_2$ClTe-*-Cl (**34**: $\Delta\theta_{\text{p:POM-M–CIV}} = -0.2°$; $\Delta\theta_{\text{p:POM-Z–CIV}} = -0.2°$), Me$_2$BrTe-*-Br (**35**: $\Delta\theta_{\text{p:POM-Z–CIV}} = -0.2°$), and Me$_2Te^+$-*-I (**45**: $\Delta\theta_{\text{p:POM-M–CIV}} = 0.6°$; $\Delta\theta_{\text{p:POM-M–Z}} = 0.6°$). The results show that the behavior of $\theta_{\text{p:POM-M}}$, $\theta_{\text{p:POM-Z}}$, and $\theta_{\text{p:CIV}}$ are the same with each other for **1–56** under MP2/S-TZPsp, although some magnitudes of $\Delta\theta_p$ amount to 0.6–0.7°. It must be the reflections of the excellent similarities in the

perturbed structures generated with POM-M, POM-Z, and CIV (see entries 1–3 in Table 2). The results lead the excellent correlations shown in Table 2 (entries 4–6).

Figure 5 displays the plots of $\kappa_{p:POM-M}$ versus $\kappa_{p:CIV}$ and $\kappa_{p:POM-Z}$ versus $\kappa_{p:CIV}$ for **1–56**, evaluated under MP2/S-TZPsp. The plots give very good correlations, again, which are presented in Table 2 (entries 7 and 8, respectively). The $\kappa_{p:POM-M}$ values are similarly plotted versus $\kappa_{p:POM-Z}$, although not shown in a figure. The plot also gives a very good correlation, which is shown in Table 2 (entry 9).

The magnitudes of $\Delta\kappa_{p:POM-M–CIV}$ (= $\kappa_{p:POM-M}$ − $\kappa_{p:CIV}$), $\Delta\kappa_{p:POM-Z–CIV}$ (= $\kappa_{p:POM-Z}$ − $\kappa_{p:CIV}$) and $\Delta\kappa_{p:POM-M–Z}$ (= $\kappa_{p:POM-M}$ − $\kappa_{p:POM-Z}$) are less than or equal to 2.5 au^{-1} for all interactions, except for Me$_2$O-*-HOH (**10**: $\Delta\kappa_{p:POM-M–CIV}$ = −10.5 au^{-1}; $\Delta\kappa_{p:POM-Z–CIV}$ = −12.0 au^{-1}), Me$_2$S-*-Cl$_2$ (**14**: $\Delta\kappa_{p:POM-M–CIV}$ = 12.0 au^{-1}; $\Delta\kappa_{p:POM-Z–CIV}$ = 7.0 au^{-1}; $\Delta\kappa_{p:POM-M–POM-Z}$ = 5.0 au^{-1}), Me$_2$S-*-Br$_2$ (**15**: $\Delta\kappa_{p:POM-M–CIV}$ = 4.7 au^{-1}; $\Delta\kappa_{p:POM-M–POM-Z}$ = 2.9 au^{-1}), Me$_2$S-*-I$_2$ (**16**: $\Delta\kappa_{p:POM-Z–CIV}$ = 5.0 au^{-1}; $\Delta\kappa_{p:POM-M–POM-Z}$ = −3.6 au^{-1}), Me$_2$Se-*-Br$_2$ (**18**: $\Delta\kappa_{p:POM-Z–CIV}$ = 3.8 au^{-1}), Me$_2$Se-*-I$_2$ (**19**: $\Delta\kappa_{p:POM-M–CIV}$ = 9.0 au^{-1}; $\Delta\kappa_{p:POM-Z–CIV}$ = 6.8 au^{-1}), Me$_2$Te-*-I$_2$ (**21**: $\Delta\kappa_{p:POM-M–POM-Z}$ = −2.6 au^{-1}), Me$_2$Te-*-I$_2$ (**22**: $\Delta\kappa_{p:POM-M–CIV}$ = 4.5 au^{-1}; $\Delta\kappa_{p:POM-M–POM-Z}$ = 3.7 au^{-1}), Me$_2$(Br)Se-*-Br (**33**: $\Delta\kappa_{p:POM-M–CIV}$ = 3.8 au^{-1}; $\Delta\kappa_{p:POM-Z–CIV}$ = 3.8 au^{-1}), and Me$_2$(Cl)Te-*-Cl (**34**: $\Delta\kappa_{p:POM-M–CIV}$ = 3.9 au^{-1}; $\Delta\kappa_{p:POM-Z–CIV}$ = 3.9 au^{-1}), Me$_2$(I)Te-*-I (**36**: $\Delta\kappa_{p:POM-M–CIV}$ = 4.0 au^{-1}; $\Delta\kappa_{p:POM-Z–CIV}$ = 4.0 au^{-1}).
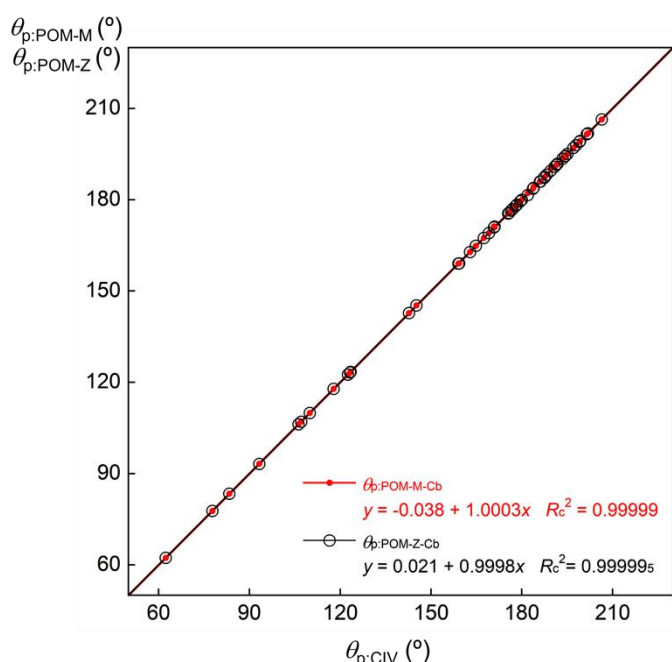
Figure 4. Plots of $\theta_{p:POM-M}$ versus $\theta_{p:CIV}$ and $\theta_{p:POM-Z}$ versus $\theta_{p:CIV}$ for **1–56**, calculated under MP2/S-TZPsp. The correlations are shown in the figure.
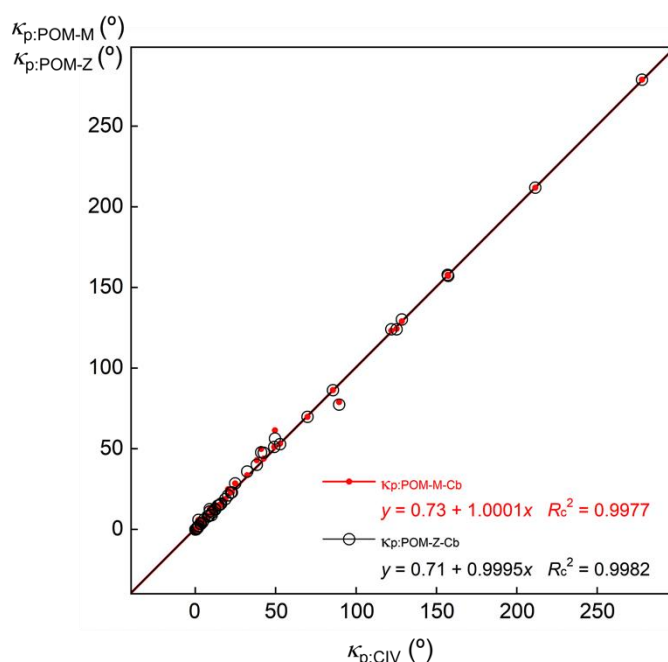
Figure 5. Plots of $\kappa_{p:POM-M}$ versus $\kappa_{p:CIV}$ and $\kappa_{p:POM-Z}$ versus $\kappa_{p:CIV}$ for **1–56**, calculated under MP2/S-TZPsp. The correlations are shown in the figure.

The high reliabilities of $\theta_{p:POM-M}$, $\theta_{p:POM-Z}$, and $\theta_{p:CIV}$ are established equally based on the excellent correlations among them. The high reliabilities of $\kappa_{p:POM-M}$, $\kappa_{p:POM-Z}$, and $\kappa_{p:CIV}$ are similarly established judging from the very good correlations. However, the reliabilities in θ_p seem higher than those in κ_p. This would be curious, at first glance, since the same perturbed structures with the common regression curve are used to evaluate θ_p and κ_p (see eq. (SA6) in the Appendix of the Supporting Information). How can the differences be explained? The differences may be mainly attributable to the much more complex route to evaluate κ_p (= $[d^2y/dx^2]/[1 + (dy/dx)^2]^{3/2}$), relative to the case of θ_p (= $90° - \tan^{-1}(dy/dx)$), as pointed out before.[37] The (very) small differences in the QTAIM functions for the perturbed structures generated with POM-M, POM-Z, and CIV

would be magnified in the second derivatives to evaluate κ_p. The process would magnify the differences more in $\kappa_{p:POM-M}$, $\kappa_{p:POM-Z}$, and $\kappa_{p:CIV}$, relative to the case in $\theta_{p:POM-M}$, $\theta_{p:POM-Z}$, and $\theta_{p:CIV}$.

The (R, θ, θ_p) parameters are employed to classify and characterize the interactions in question, whereas κ_p are not used. Therefore, the reliabilities of the predicted natures using the perturbed structures generated with POM-M, POM-Z, and CIV are clearly demonstrated to be the same with each other. The common (R, θ) parameters are employed in the processes.

Prediction of the natures for the interactions in 1–56 under MP2/S-TZPsp

The natures of the interactions in question of **1–56** are predicted based on the (R, θ, θ_p) values calculated with MP2/S-TZPsp (Table 3), under the guidance of the requirements (criteria) shown in Table 1 and the explanation in the section of "Survey of QTAIM-DFA and QTAIM approach", established for the standard interactions consisted of the atoms of the 1st–4th periods calculated with MP2/6-311++G(3df,3pd). The basic values of (θ, θ_p) described in bold are superior to the ones given tentatively in plain, in the classification and characterization of interactions. The θ_p values calculated based on the perturbed structures generated with POM-M are employed for the following discussion.

The $(\theta, \theta_{p:POM-M})$ values for A-*-HF (A = He, Ne, and Ar) are (58.9–70.3°, 62.3–83.4°), therefore, the interactions are predicted to have the vdW nature, appeared in the *p*-CS region. The nature is abbreviated by *p*-CS/vdW. However, the $(\theta, \theta_{p:POM-M})$ values are (78.9–81.3°, 106.2–109.9°) for A-*-HF (A = Kr and Xe), which are predicted to have the *p*-CS/*t*-HB$_{nc}$ nature. In the case of the HB interactions, the *p*-CS/*t*-HB$_{nc}$ nature is predicted for NN-*-HF with $(\theta, \theta_{p:POM-M})$ = (84.2°, 123.3°), HF-*-HF with $(\theta, \theta_{p:POM-M})$ = (85.8°, 117.9°), and H$_2$O-*-HOH with $(\theta, \theta_{p:POM-M})$ = (88.0°, 123.4°). The $(\theta, \theta_{p:POM-M})$ are (99.8°, 145.3°) for Me$_2$O-*-HOH and (113.0°, 159.1°) for HCN-*-HF, which are predicted to have the *r*-CS/*t*-HB$_{wc}$ and *r*-CS/CT-MC nature, respectively. For the MC adducts, the $(\theta, \theta_{p:POM-M})$ values are (79.1–84.3°, 93.2–107.2°) for Me$_2$O-*-X$_2$ (X = Cl and Br), of which nature is predicted to be *p*-CS/*t*-HB$_{nc}$, while the values are (90.3°, 122.4°) for Me$_2$O-*-I$_2$, which is predicted to have the *r*-CS/*t*-HB$_{wc}$ nature, although it is on the borderline area between the *p*-CS/*t*-HB$_{nc}$ and *r*-CS/*t*-HB$_{wc}$ nature, since the θ value of 90.3° is very close to 90.0°. The values are (118.8–138.6°, 162.8–176.9°) for Me$_2$E-*-X$_2$, (E = S, Se; X =Cl, Br, and I) of which nature is predicted to be *r*-CS/CT-MC, while the CT-TBP nature is predicted for Me$_2$Te-*-X$_2$ (X = Cl, Br, and I) with $(\theta, \theta_{p:POM-M})$ = (150.8–166.2°, 182.2–184.3°).

The *r*-CS/CT-MC nature is predicted for all X$_3^-$ in Table 3 with $(\theta, \theta_{p:POM-M})$ = (143.6–159.7°, 175.5–180.0°), except for [I-*-I$_2$]$^-$ of which nature is *r*-CS/CT-TBP, since $(\theta, \theta_{p:POM-M})$ = (159.1°, 183.8°). The *r*-CS/CT-TBP nature is predicted for all Me$_2$XE-*-X (E = S and Se; X = Cl and Br) and Me$_2$ITe-*-I with $(\theta, \theta_{p:POM-M})$ = (166.4–176.2°, 186.0–191.5°), except for Me$_2$XTe-*-X (X = Cl and Br) predicted to be *r*-CS/CT-MC nature with $(\theta, \theta_{p:POM-M})$ = (165.9–171.8°, 159.1–175.7°). In the case of Me$_2$E$^+$-*-X (E = S and Se; X = Cl, Br, and I), Me$_2$Te$^+$-*-I, and X-*-X (X = Cl, Br, and I) and H$_3$C-*-X (X = Cl, Br, and I) are all predicted to have the SS/Cov-w nature, since $(R, \theta, \theta_{p:POM-M})$ = (0.034–0.140 au, 180.1–193.9°, 178.4–199.1°), except for Me$_2$Te$^+$-*-Cl and Me$_2$Te$^+$-*-Br of which nature is predicted to be *r*-CS/*t*-HB$_{wc}$ with $(\theta, \theta_{p:POM-M})$ = (167.3°, 142.7°) and *r*-CS/CT-MC with $(\theta, \theta_{p:POM-M})$ = (178.5°, 164.9°), respectively. The SS/Cov-s nature is predicted for the classical strong chemical bonds of H$_n$C-*-CH$_n$ (n = 1–3), CH$_3$-*-H, and H-*-H, since $(R, \theta, \theta_{p:POM-M})$ = (0.237–0.648 au, 194.4–206.1°, 194.4–206.4°).

Pseudo intrinsic dynamic nature of interactions based on the perturbed structures generated with POM

The dynamic nature predicted with CIV is described as the "intrinsic dynamic nature," as aforementioned. The reliability of dynamic nature predicted with POM-M and POM-Z is demonstrated to be the same as that with CIV. The perturbed structures with POM-M and POM-Z are formulated based on the thermal process, whereas those with CIV would correspond to the adiabatic process. Therefore, the dynamic nature of interactions

predicted with POM-M and POM-Z seems unsuitable to describe as the "intrinsic dynamic nature," irrespective of the same reliability of the natures with the three methods.

We propose that the dynamic natures of interactions predicted with POM-M and POM-Z are to be describe as the "pseudo-intrinsic dynamic nature of interactions." The proposal using POM will release experimental chemists from worrying about the Compliance program, when they study their theme, concerning the chemical bonds and interactions, in more detail. It will also release from the frequency analysis of the optimized structures, where the difficulty of the frequency analysis increases as the species become larger and/or more complex.

Our aim is completely achieved to generate the perturbed structures of the same quality as that with CIV for QTAIM-DFA, by applying with POM-M and POM-Z. The slight differences between $\kappa_{p:POM}$ and $\kappa_{p:CIV}$ will not damage our discussion, since κ_p are not used to characterize the interactions, as mentioned above. Some difficulties are often encountered with POM-Z, especially when it is applied to large and/or complex species, in our experience. However, POM-M would solve the problem. POM-M seems more easily formulated and converged more effectively, than the case of POM-Z. The frequency analysis is necessary in CIV but not in POM, which is very important, especially when the method is applied to large and/or complex species at the MP2 level.

The simpler and easier method to predict the pseudo intrinsic dynamic nature of interactions, other than above, is proposed, next.

Reliability of dynamic nature with three data points versus that with five data points
A trial was made for further simplification to predict the dynamic nature of interactions. The dynamic nature for an interaction is tried for calculations by analyzing the plot for the data of the two perturbed structures and a fully optimized structure using the regression curve of a linear function. For the full analysis of the interactions with QTAIM-DFA, four perturbed structures and a fully optimized structure, with the regression curve of a cubic function, are necessary to predict the nature of an interaction. The θ_p values derived from the regression curves of cubic and linear functions are denoted by θ_{p-Cb} and θ_{p-Ln}, respectively, here. The θ_{p-Cb} and θ_{p-Ln} values are denoted as $\theta_{p-POM-M-Cb}$ and $\theta_{p-POM-M-Ln}$, respectively, if they are calculated with POM-M. Table 4 collects the $\theta_{p-POM-M-Cb}$ and $\theta_{p-POM-M-Ln}$ values for the standard interactions in **1–56**, calculated under MP2/S-TZPsp.

The reliability for $\theta_{p:POM-M-Ln}$ will be established if the $\theta_{p:POM-M-Cb}$ and $\theta_{p:POM-M-Ln}$ values are substantially the same. The $\theta_{p:POM-M-Ln}$ values are very close to the $\theta_{p:POM-M-Cb}$ values, respectively, for the same species. The magnitudes in the differences between $\theta_{p:POM-M-Ln}$ and $\theta_{p-POM-M-Cb}$ ($\Delta\theta_{p:POM-Ln-Cb} = \theta_{p:POM-M-Ln} - \theta_{p:POM-M-Cb}$) are less than or equal to 0.1° for all interactions, except for HF-∗-HF (**7**), H$_2$O-∗-HOH (**9**), Me$_2$O-∗-I$_2$ (**13**), Me$_2$Te-∗-Cl$_2$ (**20**), Me$_2$BrSe-∗-Br (**33**) and Me$_2$Se$^+$-∗-Cl (**40**), of which $\Delta\theta_{p:POM-Ln-Cb}$ values are 0.2° in magnitudes, with $\Delta\theta_{p:POM-Ln-Cb} = -0.3°$ for Me$_2$ClTe-∗-Cl (**34**).

To confirm the reliability of $\theta_{p:POM-M-Ln}$ further, the $\theta_{p-POM-M-Ln}$ values are plotted versus $\theta_{p:POM-M-Cb}$. Figure 6 shows the plot, which gives an excellent correlation. The correlation is shown in Table 2 (entry 10). The results confirm again the excellent reliability of $\theta_{p:POM-M-Ln}$. The $\theta_{p:POM-M-Ln}$ values, based on the three data points, are demonstrated to be very close to the $\theta_{p:POM-M-Cb}$ values, derived from the five data points. As a result, $\theta_{p:POM-M-Ln}$ can be employed for the discussion of high reliability, in place of $\theta_{p:POM-M-Cb}$. The results show that the reliability of $\theta_{p:POM-M-Ln}$ is the same as that of $\theta_{p:POM-M-Cb}$. The results also show that the dynamic nature derived from the three data points calculated with POM-M retains the very high reliability very close to that derived from the five data points calculated with POM-M. Namely, the dynamic nature based on the three data points

with POM-M can be used with the very high reliability. The reliability of $\theta_{p:POM-M-Ln}$ can be recognized as substantially the same as that of $\theta_{p:ClV-Cb}$ through $\theta_{p:POM-M-Cb}$.

Table 4. The θ, $\theta_{p:POM-M-Cb}$, $\theta_{p:POM-M-Ln}$, and $\theta_{p:OMA-Ln}$ values for the Standard Interactions in **1–56**, Calculated with QTAIM-DFA under MP2/S-TZPsp, where the Perturbed Structures being Generated with POM-M and OMA[a–c]

X-*-Y (Species: No)	$\theta_{p:POM-M-Cb}$ (°)	$\theta_{p:POM-M-Ln}$ (°)	$\theta_{p:OMA-Ln}$ (°)	Predicted Nature	X-*-Y (Species: No)	$\theta_{p:POM-M-Cb}$ (°)	$\theta_{p:POM-M-Ln}$ (°)	$\theta_{p:OMA-Ln}$ (°)	Predicted Nature
He-*-HF (**1**)	62.3	62.4	62.4	*p*-CS/vdW	[Br-*-IBr]⁻ (**29**)	180.0	180.0	178.9	*r*-CS/CT-MC
Ne-*-HF (**2**)	77.8	77.8	77.8	*p*-CS/vdW	Me₂ClS-*-Cl (**30**)	191.5	191.6	191.3	*r*-CS/CT-TBP
Ar-*-HF (**3**)	83.4	83.4	83.4	*p*-CS/vdW	Me₂BrS-*-Br (**31**)	187.3	187.4	187.5	*r*-CS/CT-TBP
Kr-*-HF (**4**)	106.2	106.3	106.2	*p*-CS/*t*-HBₙc	Me₂ClSe-*-Cl (**32**)	187.4	187.4	186.8	*r*-CS/CT-TBP
Xe-*-HF (**5**)	109.9	110.0	109.9	*p*-CS/*t*-HBₙc	Me₂BrSe-*-Br (**33**)	186.0	186.2	185.8	*r*-CS/CT-TBP
NN-*-HF (**6**)	123.3	123.4	123.2	*p*-CS/*t*-HBₙc	Me₂ClTe-*-Cl (**34**)	159.1	158.8	158.0	*r*-CS/CT-MC
HF-*-HF (**7**)	117.9	118.1	116.4	*p*-CS/*t*-HBₙc	Me₂BrTe-*-Br (**35**)	175.7	175.6	174.9	*r*-CS/CT-MC
HCN-*-HF (**8**)	159.1	159.1	158.1	*r*-CS/CT-MC	Me₂ITe-*-I (**36**)	187.5	187.5	187.2	*r*-CS/CT-TBP
H₂O-*-HOH (**9**)	123.4	123.6	123.4	*p*-CS/*t*-HBₙc	Me₂S⁺-*-Cl (**37**)	197.9	197.9	198.0	SS/Cov-w
Me₂O-*-HOH (**10**)	145.3	145.3	142.1	*r*-CS/*t*-HBwc	Me₂S⁺-*-Br (**38**)	195.1	195.1	195.2	SS/Cov-w
Me₂O-*-Cl₂ (**11**)	93.2	93.3	93.7	*p*-CS/*t*-HBₙc	Me₂S⁺-*-I (**39**)	178.4	178.3	178.8	SS/Cov-w
Me₂O-*-Br₂ (**12**)	107.2	107.3	107.8	*p*-CS/*t*-HBₙc	Me₂Se⁺-*-Cl (**40**)	186.0	185.8	185.9	SS/Cov-w
Me₂O-*-I₂ (**13**)	122.4	122.6	123.7	*r*-CS/*t*-HBwc	Me₂Se⁺-*-Br (**41**)	193.5	193.5	193.6	SS/Cov-w
Me₂S-*-Cl₂ (**14**)	162.8	162.9	159.5	*r*-CS/CT-MC	Me₂Se⁺-*-I (**42**)	188.3	188.2	188.5	SS/Cov-w
Me₂S-*-Br₂ (**15**)	167.4	167.5	165.9	*r*-CS/CT-MC	Me₂Te⁺-*-Cl (**43**)	142.7	142.7	142.7	*r*-CS/*t*-HBwc
Me₂S-*-I₂ (**16**)	169.1	169.1	168.6	*r*-CS/CT-MC	Me₂Te⁺-*-Br (**44**)	164.9	164.8	164.8	*r*-CS/CT-MC
Me₂Se-*-Cl₂ (**17**)	176.9	177.0	174.0	*r*-CS/CT-MC	Me₂Te⁺-*-I (**45**)	190.2	190.1	189.7	SS/Cov-w
Me₂Se-*-Br₂ (**18**)	170.9	171.0	169.4	*r*-CS/CT-MC	Cl-*-Cl (**46**)	194.3	194.3	194.3	SS/Cov-w
Me₂Se-*-I₂ (**19**)	171.3	171.2	170.1	*r*-CS/CT-MC	Br-*-Br (**47**)	191.8	191.8	191.8	SS/Cov-w
Me₂Te-*-Cl₂ (**20**)	184.3	184.1	183.8	*r*-CS/CT-TBP	I-*-I (**48**)	190.9	190.9	190.9	SS/Cov-w
Me₂Te-*-Br₂ (**21**)	183.7	183.7	183.1	*r*-CS/CT-TBP	CH₃-*-Cl (**49**)	199.1	199.1	198.8	SS/Cov-w
Me₂Te-*-I₂ (**22**)	182.2	182.2	181.2	*r*-CS/CT-TBP	CH₃-*-Br (**50**)	197.0	197.0	196.8	SS/Cov-w
[Cl-*-Cl₂]⁻ (**23**)	178.4	178.5	177.3	*r*-CS/CT-MC	CH₃-*-I (**51**)	179.5	179.4	179.8	SS/Cov-w
[Br-*-Br₂]⁻ (**24**)	176.5	176.6	175.3	*r*-CS/CT-MC	CH₃-*-CH₃ (**52**)	201.8	201.8	201.7	SS/Cov-s
[I-*-I₂]⁻ (**25**)	183.8	183.8	182.7	*r*-CS/CT-TBP	CH₂-*-CH₂ (**53**)	199.3	199.3	199.4	SS/Cov-s
[Cl-*-BrCl]⁻ (**26**)	179.9	180.0	178.6	*r*-CS/CT-MC	CH-*-CH (**54**)[d]	194.4	194.4	194.4	SS/Cov-s
[Br-*-ClBr]⁻ (**27**)	175.5	175.6	174.7	*r*-CS/CT-MC	CH₃-*-H (**55**)	201.5	201.4	201.3	SS/Cov-s
[Cl-*-ICl]⁻ (**28**)	177.9	177.8	176.7	*r*-CS/CT-MC	H-*-H (**56**)	206.4	206.4	206.4	SS/Cov-s

[a] Data are given for the interaction in question at the BCP, which is shown by He-*-HF, for an example. [b] $\theta_p = 90° - \tan^{-1}(\mathrm{d}y/\mathrm{d}x)$, where $(x, y) = (H_b(r_c) - V_b(r_c)/2, H_b(r_c))$. [c] Cb in $\theta_{p:POM-M-Cb}$, and Ln in $\theta_{p:POM-M-Ln}$ stand for the cubic and linear functions, respectively, as the regression curves (*cf*: eqs. (6) and (7)). [d] Data from $w = 0$, ±0.025, and ±0.5 were employed, since the (3, –3) attractor appeared at the center of the perturbed structure for $w = -0.1$.

Reliability of dynamic nature with three data points using perturbed structurers generated by OMA

The simplification was further examined. The perturbed structures are generated with OMA, the ultimate method, where the major interactions are only fixed appropriately longer and shorter than those in the optimized structures. (No further optimizations are made for the perturbed structures in OMA.) In this work, the θ_p value for an interaction was calculated by analyzing the regression curve of a linear function for the plot

of the data from the two perturbed structures and the fully optimized structures. The θ_p value is named $\theta_{p:OMA-Ln}$. Table 4 collects the $\theta_{p:OMA-Ln}$ values calculated under MP2/S-TZPsp. The $\theta_{p:OMA-Ln}$ values are very close to the $\theta_{p:POM-M-Cb}$ values, respectively, for the same species. The magnitudes in the differences between $\theta_{p:OMA-Ln}$ and $\theta_{p:POM-M-Cb}$ ($\Delta\theta_{p:POM-Ln-Cb} = \theta_{p:OMA-Ln} - \theta_{p:POM-M-Cb}$) are less than or equal to 1.5° for all interactions, except for Me$_2$O-*-HOH (**10**), Me$_2$S-*-Cl$_2$ (**14**), and Me$_2$Se-*-Cl$_2$ (**17**), of which $\Delta\theta_{p:POM-Ln-Cb}$ values are −3.2°, −3.3°, and −2.9°, respectively. Among the interactions with $\Delta\theta_{p:POM-Ln-Cb}$ less than or equal to 1.5°, The $\Delta\theta_{p:POM-Ln-Cb}$ values are less than or equal to 1.0° for **41** interactions and less than or equal to 1.5° for **12** interactions. The magnitudes of $\Delta\theta_{p:POM-Ln-Cb}$ seem large when the minor interactions are placed just the backside of the major ones. Namely the three atoms in the major and minor interactions are aligned linearly. In such case, the minor interactions will be affected much from the major ones, in the calculation process.
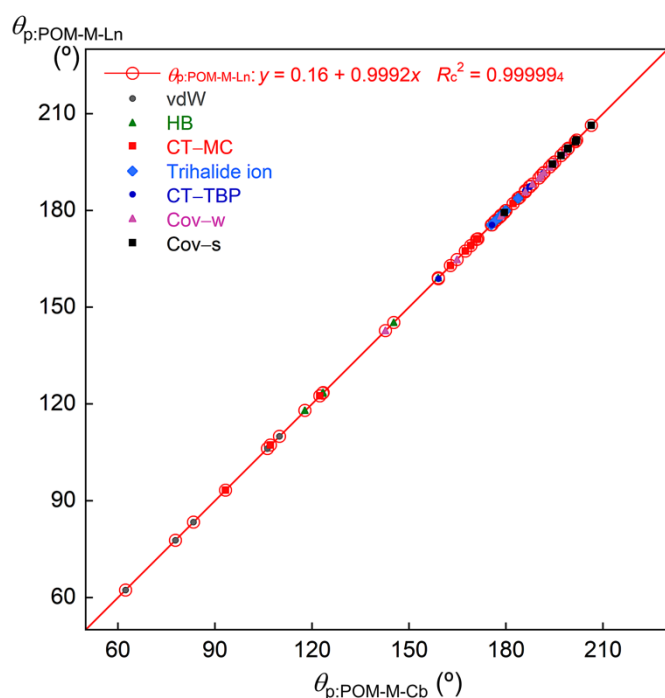
Figure 6. Plots of $\theta_{p:POM-M-Ln}$ versus $\theta_{p:POM-M-Cb}$, calculated with MP2/S-TZPsp. The correlation is shown in the figure. Colors for the interactions are the same as those in Table 3.
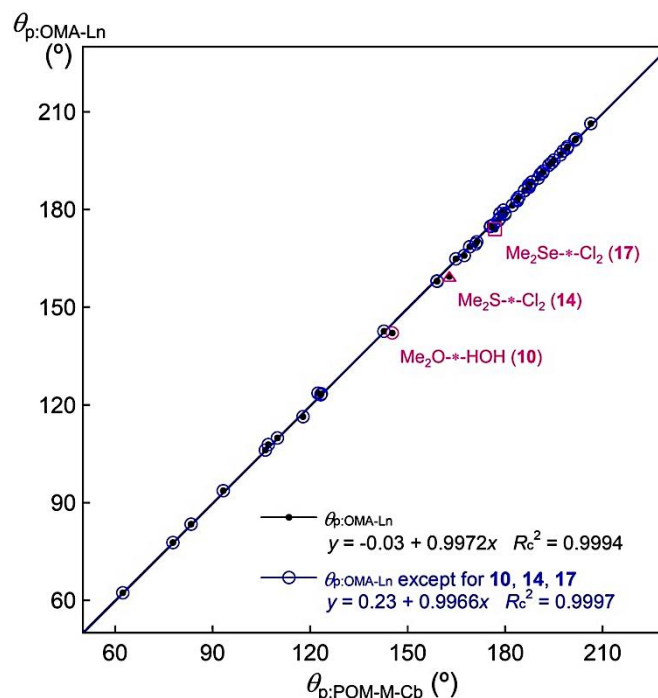
Figure 7. Plots of $\theta_{p:OMA-Ln}$ versus $\theta_{p:POM-M-Cb}$, calculated under MP2/S-TZPsp. Correlations are shown in the figure, where the data for Me$_2$O-*-HOH (**10**), Me$_2$S-*-Cl$_2$ (**14**), and Me$_2$Se-*-Cl$_2$ (**17**) being omitted in the blue one.

Figure 7 shows the plot of $\theta_{p:OMA-Ln}$ versus $\theta_{p:POM-M-Cb}$, which gives an excellent correlation. The correlation is shown in Table 2 (entry 11). The correlation is also calculated by omitting the data from Me$_2$O-*-HOH (**10**), Me$_2$S-*-Cl$_2$ (**14**), and Me$_2$Se-*-Cl$_2$ (**17**). The correlation is also shown in Table 2 (entry 12). The $\theta_{p:OMA-Ln}$ values, based on the three data points, are demonstrated to be very close to the $\theta_{p:POM-M-Cb}$ values, which are derived from the five data points. The results confirm again the very high reliability of $\theta_{p:POM-M-Ln}$.

As a result, $\theta_{p:OMA-Ln}$ can also be employed for the discussion with high reliability, in place of $\theta_{p:POM-M-Cb}$. The $\theta_{p:OMA-Ln}$ values will be effectively applied to very lsrge and/or complex species, containing the biological species.

Applications of the proposed methodology to noncovalent ^{1}E---^{2}E, ^{1}E---^{2}E=O, O=^{1}E---^{2}E, and O=^{1}E---^{2}E=O (^{1}E, ^{2}E = S, Se) interactions

The proposed simpler and easier methods of OMA-Ln and POM-M-Ln are applied, together with CIV-Ln, POM-M-Cb and CIV-Cb, to the noncovalent ^1E---^2E, ^1E---^2E=O, O=^1E---^2E, and O=^1E---^2E=O (^1E, ^2E = S, Se) interactions at the naphthalene 1,8-positions of **57a**–**59c**[38,39] with QTAIM-DFA under MP2/S-TZPsp (Chart 1).
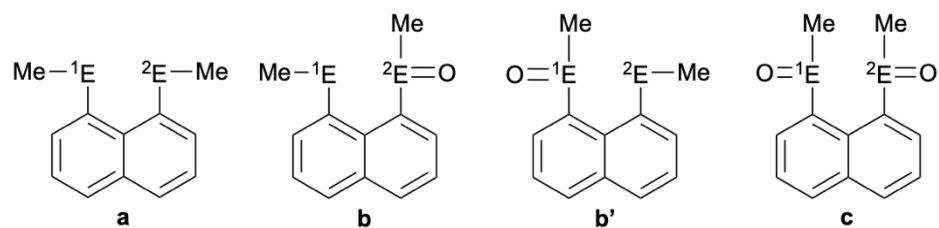

Chart 1. Structures of **57a**–**59c**.

Figure 8 shows the observed structures of **59a**–**59c**.[39] The structures of **57a**–**59c** are optimized under MP2/S-TZPsp, which are shown in Figure S3 of the Supporting Information. The observed structures are well reproduced by the optimizations, as shown in Table S4 of the Supporting Information. Figure 9 illustrates the molecular graphs of the species, exemplified by **59a**–**59c**. The molecular graphs, other than **59a**–**59c**, are shown in Figure S4 of the Supporting Information. All BPs with BCP are clearly detected, containing those for the noncovalent ^1E-*-^2E interactions.
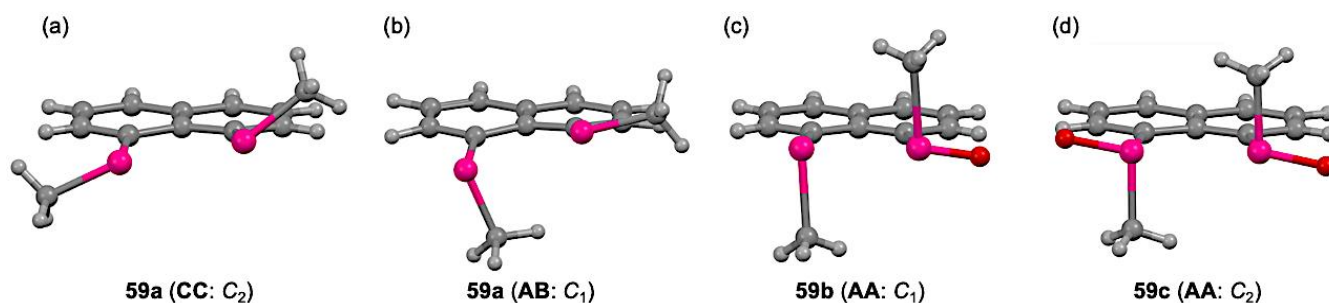
Figure 8. Observed structures of **59a** (**CC**) (a), **59b** (**AA**), and **59c** (**AA**) (d), together with optimized structure of **59a** (**AB**) (b).
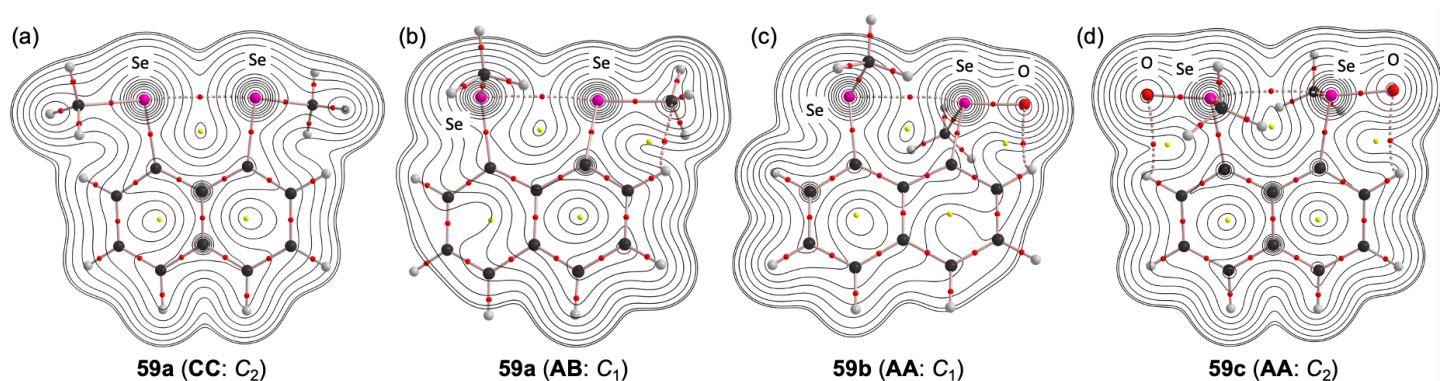
Figure 9. Molecular graphs with the counter plots for **59a** (**CC**) (a), **59a** (**AB**) (b), **59b** (**AA**) (c), and **59c** (**AA**) (d), drawn under MP2/S-TZPsp. BCPs are denoted by red dots, RCP (ring critical points) by yellow dots and BPs by pink lines. Carbon, hydrogen, selenium, and oxygen atoms are shown in black, grey, pink, and red, respectively.

Contour plots are drawn on the planes containing ^{1}E-∗-^{2}E interaction. The contours (ea_o^{-3}) are at 2^I ($I = \pm 8$, ± 7, ... and 0). Types for **AA**, **AB**, and **CC** are defined in Scheme S1b of the Supporting Information.

Table 5 collects the R, θ, and θ_p ($\theta_{p:OMA-Ln}$, $\theta_{p:POM-M-Ln}$, $\theta_{p:POM-M-Cb}$, $\theta_{p:CIV-Ln}$, and $\theta_{p:CIV-Cb}$) values, obtained under MP2/S-TZPsp, together with the predicted natures. The QTAIM functions and QTAIM-DFA parameter of $\rho_b(r_c)$, $\nabla^2\rho_b(r_c)$, and $H_b(r_c) - V_b(r_c)/2$, $H_b(r_c)$ values are given in Table S5 of the Supporting Information. The interactions in Table 5 are all predicted to have the r-CS/t-HB$_{wc}$ nature based on all methods.

The magnitudes in the deviations of $\theta_{p:POM-M-Ln}$ and $\theta_{p:CIV-Ln}$ (and $\theta_{p:POM-M-Cb}$) from $\theta_{p:CIV-Cb}$ are less than 0.1° for all interactions, except for $\theta_{p:POM-M-Ln}$ and $\theta_{p:POM-M-Cb}$ for O=S-∗-S=O (**57c**) and $\theta_{p:POM-M-Cb}$ for O=S-∗-Se=O (**58c**), of which magnitudes are 0.2°. It is demonstrated that $\theta_{p:POM-M-Ln}$ and $\theta_{p:CIV-Ln}$ (and $\theta_{p:POM-M-Cb}$) can be widely applied to predict the natures of interactions in the usual molecules, such as **57a–59c**, with the excellently high reliability, in addition to $\theta_{p:CIV-Cb}$, again.

Table 5. QTAIM-DFA Parameters of the R, θ, and θ_p values for the noncovalent ^{1}E---^{2}E, ^{1}E---^{2}E=O, O=^{1}E---^{2}E, and O=^{1}E---^{2}E=O (^{1}E, ^{2}E = S, Se) Interactions at the Naphthalene 1,8-Positions Calculated with QTAIM-DFA by employing the OMA-Ln, POM-M-Ln, CIV-Ln, POM-M-Cb, and CIV-Cb methods under MP2/S-TZPsp^{a-d}

Species (X-∗-Y) (No: symmetry)	R (au)	θ (°)	$\theta_{p:OMA-Ln}$ (°)	$\theta_{p:POM-M-Ln}$ (°)	$\theta_{p:CIV-Ln}$ (°)	$\theta_{p:POM-M-Cb}$ (°)	$\theta_{p:CIV-Cb}$ (°)	Predicted nature
S-∗-S (**57a**: **CC** (C_2))	0.0079	93.2	120.9	119.4	119.5	119.4	119.4	r-CS/t-HB$_{wc}$
S-∗-S (**57a**: **AB** (C_1))	0.0071	95.6	126.8	126.5	126.3	e	126.2	r-CS/t-HB$_{wc}$
S-∗-S=O (**57b**: **AA** (C_1))	0.0063	95.8	125.9	125.5	125.6	125.5	125.5	r-CS/t-HB$_{wc}$
O=S-∗-S=O (**57c**: **AA** (C_2))	0.0058	91.4	116.3	116.8	116.7	116.8	116.6	r-CS/t-HB$_{wc}$
S-∗-Se (**58a**: **AB** (C_1))	0.0072	99.4	134.0	133.4	133.3	133.4	133.3	r-CS/t-HB$_{wc}$
S-∗-Se=O (**58b**: **AA** (C_1))	0.0064	99.8	133.2	132.7	132.7	132.6	132.6	r-CS/t-HB$_{wc}$
Se-∗-S=O (**58b'**: **AA** (C_1))	0.0057	97.6	124.8	124.8	124.8	124.7	124.7	r-CS/t-HB$_{wc}$
O=S-∗-Se=O (**58c**: **AA** (C_1))	0.0057	93.1	118.2	118.2	118.4	118.1	118.3	r-CS/t-HB$_{wc}$
Se-∗-Se (**59a**: **CC** (C_2))	0.0069	97.2	126.6	123.2	123.1	123.2	123.1	r-CS/t-HB$_{wc}$
Se-∗-Se (**59a**: **AB** (C_1))	0.0064	100.6	131.6	131.4	130.9	e	130.8	r-CS/t-HB$_{wc}$
Se-∗-Se=O (**59b**: **AA** (C_1))	0.0058	102.6	132.5	132.0	132.1	131.9	132.0	r-CS/t-HB$_{wc}$
O=Se-∗-Se=O (**59c**: **AA** (C_2))	0.0052	94.4	117.3	118.0	118.0	118.0	117.9	r-CS/t-HB$_{wc}$

^{a} See Table 4 and text for the OMA-Ln, POM-M-Ln, CIV-Ln, POM-M-Cb, and CIV-Cb methods. ^{b} $R = (x^2 + y^2)^{1/2}$, where (x, y) = $(H_b(r_c) - V_b(r_c)/2, H_b(r_c))$. ^{c} $\theta = 90° - \tan^{-1}(y/x)$. ^{d} $\theta_p = 90° - \tan^{-1}(dy/dx)$. ^{e} Not calculated.

In the case of $\theta_{p:OMA-Ln}$, the magnitudes in the differences between $\theta_{p:OMA-Ln}$ and $\theta_{p:CIV-Cb}$ are less than 0.7° for all interactions, except for S-∗-S (**57a** (**CC**: C_2)) and Se-∗-Se (**59a** (**CC**: C_2)) of which magnitudes are 1.5° and 3.5°, respectively. The magnitudes are reduced to 0.6° and 0.8°, respectively, if the **AB** conformers are calculated for **57a** (C_1) and **59a** (C_1) (**57a**&**59a** (**AB**: C_1)). Why the differences between $\theta_{p:OMA-Ln}$ and $\theta_{p:CIV-Cb}$ in **CC** (C_2) are larger than the case in **AB** (C_1)? The differences in perturbed structures generated with OMA and CIV must be responsible for energy surface around ^{1}E-∗-^{2}E of **57a** and **59a**. The **CC** (C_2) conformer should have unique energy surface, which must affect much on the perturbed structures. The vibrational motions corresponding to compliance force constants for ^{1}E-∗-^{2}E of **57a** (**CC**: C_2), **57a** (**AB**: C_1), **59a** (**CC**: C_2), and **59a** (**AB**: C_1), are illustrated in Figure S5 of the Supporting Information. As shown in the figure, whereas the ^{1}E-∗-^{2}E stretch in the ^{1}E-^{2}E-C direction mainly contributes to of (**AB**: C_1), lots of stretches, other than the ^{1}E-∗-^{2}E

stretch in the ^{1}E-^{2}E-C direction seem to contribute in (**CC**: C_2). As a result, the energy surface around ^{1}E-∗-^{2}E would be very different between those of **AB** and **CC**.

The reason for the calculated results in **57a**&**59a** (**AB**: C_1) versus **57a**&**59a** (**CC**: C_2) would be clarified by considering the style of the ^{1}E-∗-^{2}E interactions. The style was examined based on the NBO analysis.[40] The results of the NBO analysis for **57a**–**59c** are summarized in Table S6 of the Supporting Information. It is noteworthy that the $n_p(^1E) \rightarrow \sigma*(^2E-C_{Me})$ interaction mainly contributes to (**AB**: C_1), as expected, whereas the $n_s(^1E) \rightarrow \sigma*(^2E-C_{Me})$ interaction contributes substantially to (**CC**: C_2). The perturbed structures should be close to the optimized structure in (**AB**: C_1), since the $n_p(^1E) \rightarrow \sigma*(^2E-C_{Me})$ interaction will maintain the perturbed structures close to the optimized structure in (**AB**: C_1). On the other hand, the $n_s(^1E) \rightarrow \sigma*(^2E-C_{Me})$ interaction in (**CC**: C_2) will have less tendency to keep the perturbed structures, close to the optimization structure, since the atomic s orbital has no direction. As a result, the perturbed structures in (**AB**: C_1) will be substantially the same as the optimized structure, irrespective of the calculation methods, however, those in (**CC**: C_2) will be somewhat different with each other, depending on the calculation methods. Only the interaction distance of ^{1}E-∗-^{2}E changes in the perturbed structures, if they are generated with OMA. Namely, the perturbed structures generated with OMA will be very similar to the optimized structures in (**AB**: C_1) and (**CC**: C_2). However, the differences in the perturbed structures generated with (NIV, CIV, and POM) and OMA will be (much) larger in (**CC**: C_2), relative to the case in (**AB**: C_1), since all bond distances, containing ^{1}E-∗-^{2}E, will change in the perturbed structures, if generated with NIV, CIV, and POM. This is the reason for the much larger differences of the magnitudes between $\theta_{p:OMA-Ln}$ and $\theta_{p:CIV-Cb}$ in (**CC**: C_2), relative to the case in (**AB**: C_1), shown in Table 5.

The above discussion is to explain the larger differences of the magnitudes between $\theta_{p:OMA-Ln}$ and $\theta_{p:CIV-Cb}$ in (**CC**: C_2), relative to the case in (**AB**: C_1), which would be independent in the stability of (**AB**: C_1) and (**CC**: C_2). The stability of the conformers can be discussed based on the $E(2)$ values. As shown in Table S6 of the Supporting Information, the $E(2)$ value for $n_{s+p}(S) \rightarrow \sigma*(S-C_{Me})$ of **57a** (**CC**: C_2) is 6.80 kcal mol^{-1} ((2.85+0.55)x2), which is somewhat larger than the value of 5.71 kcal mol^{-1} for **57a** (**AB**: C_1). Similarly, the $E(2)$ value for $n_{s+p}(Se) \rightarrow \sigma*(Se-C_{Me})$ of **59a** (**CC**: C_2) is 11.76 kcal mol^{-1} ((2.53+3.35)x2), which is somewhat larger than the value of 10.59 kcal mol^{-1} (0.73+9.86) for **59a** (**AB**: C_1), again. The results predict that **57a** and **59a** (**CC**: C_2) are somewhat more stable than **57a** and **59a** (**AB**: C_1), respectively. The observed structures of **57a** and **59a** (**CC**: C_2) are well understood based on the $E(2)$ values.

The results imply that the applicability and the reliability of $\theta_{p:OMA-Ln}$ will also be very high, if the specific cases, such as the **CC** (C_2), are carefully considered, as discussed above. The $\theta_{p:OMA-Ln}$ value is expected to be applied to large molecules, such as biomolecules, although some devices would be necessary.

Conclusions

In QTAIM-DFA, the signs of $d(H_b(r_c) - V_b(r_c)/2)/dr$ and $dH_b(r_c)/dr$ (r: the interaction distance) are employed to predict the dynamic and static natures of interactions, in addition to those of $H_b(r_c) - V_b(r_c)/2$ and $H_b(r_c)$. The prediction is achieved by analyzing the QTAIM-DFA plots of $H_b(r_c)$ versus $H_b(r_c) - V_b(r_c)/2$ with (R, θ) and (θ_p, κ_p). The treatment enables us to classify and characterize the CS interactions of vdW, t-HB$_{nc}$, t-HB$_{wc}$, CT-MC, X$_3^-$, and CT-TBP, and the SS interactions of Cov-w and Cov-s. The reliability of the dynamic nature is controlled by the quality of the perturbed structures. The perturbed structures generated with CIV has been demonstrated to have the excellent quality for QTAIM-DFA. However, it seems difficult to handle freely the compliance program, necessary to operate CIV, for non-specialists in this field. We searched for the simpler and easier

methods to generate the perturbed structures, of which quality is substantially the same as that with CIV. The perturbed structures generated with POM (POM-M and POM-Z) are shown to satisfy the requirements. The dynamic nature of interactions with POM is described as the "pseudo-intrinsic dynamic nature of interactions," after the "intrinsic dynamic nature of interactions," with CIV. As an ultimate method, OMA is proposed to generate the perturbed structures, of which quality seems very good. In the full treatment of QTAIM-DFA, data from the fully optimized structure with four perturbed structures around it are analyzed, employing the regression curve of a cubic function, which is sometimes troublesome. Data from a fully optimized and two perturbed structures with the regression curve of a linear type are demonstrated to give the same reliability of the dynamic nature for an interaction as that derived from the five data points. The applicability of the proposed methods is examined, employing the noncovalent interactions at the naphthalene 1,8-positions.

The "pseudo-intrinsic dynamic nature of interactions" is obtained with POM, which helps us to predict the highly reliable dynamic nature for the interactions. In this case, the frequency analysis is not necessary. It will release the experimental chemists from worrying about the complex compliance program in CIV, when they study their theme, concerning the chemical bonds and interactions, in more detail. Analyzing the data from the three points will also release chemists from excessive effort. OMA is expected to open the door to apply QTAIM-DFA to large molecules, such as the biomolecules, although some devices would be necessary.

Supplementary Material

Additional figures, tables, schemes, and compound geometries derived from quantum chemical calculations have been submitted along with the manuscript.

References

1. *Molecular Interactions. From van der Waals to Strongly Bound Complexes*, Scheiner, S., Ed.; Wiley: New York, 1997, ch. 4–6.
https://doi.org/10.1016/S0022-2860(98)00314-7
2. Dessent, C. E. H.; Müller-Dethlefs, K. *Chem. Rev.* **2000**, *100*, 3999–4021.
https://doi.org/10.1021/cr990060r
3. Wormer, P. E. S.; van der Avoird, A. *Chem. Rev.* **2000**, *100*, 4109–4144.
https://doi.org/10.1021/cr990046e
4. *Hydrogen Bonding – A Theoretical Perspective*, Scheiner, S., Ed.; Oxford University Press: New York, 1997.
https://doi.org/10.1021/ja9756735
5. *The Weak Hydrogen Bond in Structural Chemistry and Biology; International Union of Crystallography Monographs on Crystallography*, Desiraju, G. R.; Steiner, T. Eds.; Oxford University Press: New York, 1999.
https://doi.org/10.1021/ja0047368
6. *Hydrogen Bonding: New Insights (Challenges and Advances in Computational Chemistry and Physics)* Grabowski, S. J. Ed.; Springer: The Netherlands, 2006, Vol. 3.
https://doi.org/10.1007/978-1-4020-4853-1

7. Han, K.-L.; Zhao, G.-J. *Hydrogen Bonding and Transfer in the Excited State*, Wiley: Chichester, UK, 2010.
https://doi.org/10.1002/9780470669143

8. Espinosa, E.; Lecomte, C.; Molins. E. *Chem. Phys. Lett.* **1999**, *300*, 745–748.
https://doi.org/10.1016/s0009-2614(98)01399-2

9. Espinosa, E.; Alkorta, I.; Rozas, I.; Elguero, J.; Molins, E. *Chem. Phys. Lett.* **2001**, *336*, 457–461.
https://doi.org/10.1016/s0009-2614(01)00178-6

10. Nishio, M. *Cryst. Eng. Commun.* **2004**, *6*, 130–158.
https://doi.org/10.1039/b313104a

11. Nishide, T.; Hayashi, S.; Nakanishi, W. *ChemistryOpen* **2018**, *7*, 565–575.
https://doi.org/10.1002/open.201800051

12. Nakanishi, W.; Hayashi, S.; Nishide, T. *RSC Adv.* **2020**, *10*, 24730–24742.
https://doi.org/10.1039/d0ra01357a

13. *Chemistry of Hypervalent Compounds*, Akiba, K.-Y. Ed.; Wiley-VCH, New York 1999.
https://doi.org/10.1021/ja995694u

14. Nakanishi, W. in *Hypervalent Chalcogen Compounds* In *Handbook of Chalcogen Chemistry: New Perspectives in Sulfur, Selenium and Tellurium*, Devillanova, F. A. Ed.; Royal Society of Chemistry: Cambridge 2006; ch. 10.3, pp. 644–668.
https://doi.org/10.1039/9781847557575-00644

15. Nakanishi, W.; Hayashi, S. In *Handbook of Chalcogen Chemistry: New Perspectives in Sulfur, Selenium and Tellurium* 2nd Ed., Vol 2, Devillanova, F. A.; du Mont, W.-W. Eds.; Royal Society of Chemistry: Cambridge 2013, ch. 12.3, pp. 335–372.
https://doi.org/10.1039/9781849737463-00335

16. Nakanishi, W.; Hayashi, S.; Hashimoto, M.; Arca, M.; Aragoni, M. C.; Lippolis, V. In *The Chemistry of Organic Selenium and Tellurium Compounds*, Rappoport, Z. Ed.; Wiley, New York 2014, ch. 11, vol. 4, pp. 885–972.
https://doi.org/10.1002/9780470682531.pat0701

17. *Atoms in Molecules. A Quantum Theory*, Bader, R. F. W. Ed.; Oxford University Press: Oxford, UK, 1990. [ISBN-13: 978-0198558651]

18. *An Introduction to the Quantum Theory of Atoms in Molecules In The Quantum Theory of Atoms in Molecules: From Solid State to DNA and Drug Design*, Matta, C. F.; Boyd, R. J. Eds.; WILEY-VCH, Weinheim, Germany, 2007, ch. 1.
https://doi.org/10.1002/9783527610709.ch1

19. Nakanishi, W.; Hayashi, S.; Narahara, K. *J. Phys. Chem. A* **2008**, *112*, 13593–13599.
https://doi.org/10.1021/jp8054763

20. Nakanishi, W.; Hayashi, S.; Narahara, K. *J. Phys. Chem. A* **2009**, *113*, 10050–10057.
https://doi.org/10.1021/jp903622a

21. Nakanishi, W.; Hayashi, S. *Curr. Org. Chem.* **2010**, *14*, 181–197.
https://doi.org/10.2174/138527210790069820

22. Nakanishi, W.; Hayashi, S. *J. Phys. Chem. A* **2010**, *114*, 7423–7430.
https://doi.org/10.1021/jp104278j

23. Nakanishi, W.; Hayashi, S.; Matsuiwa, K.; Kitamoto, M. *Bull. Chem. Soc. Jpn.* **2012**, *85*, 1293–1305.
https://doi.org/10.1246/bcsj.20110377

24. Nakanishi, W.; Hayashi, S. *J. Phys. Chem. A* **2013**, *117*, 1795–1803.
https://doi.org/10.1021/jp3095566

25. BCP is a point along the bond path (BP) at the interatomic surface where the electron density $\rho(\mathbf{r})$ reaches a minimum, while it is a maximum on the interatomic surface separating the atomic basins.

26. Nakanishi, W.; Hayashi, S. *Int. J. Quantum Chem.* **2018**, *118*, e25590. https://doi.org/10.1002/qua.25590

27. The C_{ij} are defined as the partial second derivatives of the potential energy due to an external force, as shown in eq. (R1), where *i* and *j* refer to internal coordinates, and the external force components acting on the system f_i and f_j correspond to *i* and *j*, respectively.
    $C_{ij} = \partial^2 E/\partial f_i \partial f_j$ (R1)
    The C_{ij} values and the coordinates corresponding to C_{ii} were calculated by using the Compliance 3.0.2 program released by J. Grunenberg and K. Brandhorst, http://www.oc.tu-bs.de/Grunenberg/compliance.html (accessed on 1st September 2022).

28. The optimizations do not converge effectively to the perturbed structures. The postulated symmetry will be often broken during the optimizations.

29. *Gaussian 09, Revision D.01*, Frisch, M. J.; Trucks, G. W.; Schlegel, H. B.; Scuseria, G. E.; Robb, M. A.; Cheeseman, J. R.; Scalmani, G.; Barone, V.; Mennucci, B.; Petersson, G. A.; Nakatsuji, H.; Caricato, M.; Li, X.; Hratchian, H. P.; Izmaylov, A. F.; Bloino, J.; Zheng, G.; Sonnenberg, J. L.; Hada, M.; Ehara, M.; Toyota, K.; Fukuda, R.; Hasegawa, J.; Ishida, M.; Nakajima, T.; Honda, Y.; Kitao, O.; Nakai, H.; Vreven, T.; Montgomery, Jr., J. A.; Peralta, J. E.; Ogliaro, F.; Bearpark, M.; Heyd, J. J.; Brothers, E.; Kudin, K. N.; Staroverov, V. N.; Kobayashi, R.; Normand, J.; Raghavachari, K.; Rendell, A.; Burant, J. C.; Iyengar, S. S.; Tomasi, J.; Cossi, M.; Rega, N.; Millam, J. M.; Klene, M.; Knox, J. E.; Cross, J. B.; Bakken, V.; Adamo, C.; Jaramillo, J.; Gomperts, R.; Stratmann, R. E.; Yazyev, O.; Austin, A. J.; Cammi, R.; Pomelli, C.; Ochterski, J. W.; Martin, R. L.; Morokuma, K.; Zakrzewski, V. G.; Voth, G. A.; Salvador, P.; Dannenberg, J. J.; Dapprich, S.; Daniels, A. D.; Farkas, Ö.; Foresman, J. B.; Ortiz, J. V.; Cioslowski, J.; Fox, D. J. Gaussian, Inc., Wallingford CT, 2009.

30. Noro, T.; Sekiya, M.; Koga, T. *Theor. Chem. Acc.* **2012**, *131*, 1124. https://doi.org/10.1007/s00214-012-1124-z

31. Recently, the Sapporo basis sets series can also be obtained from Basis Set Exchange, while those with the 1s1p diffusion functions are not implemented.

32. The (7433211/743111/7411/2 + 1s1p) type is employed for Te and I, for example.

33. It is desirable if the differences between the calculated and observed distances are less than 0.013 Å (= $0.05a_0/2$) in magnitude. The difference of less than around 0.03 Å (= $0.05a_0$) in magnitude would be acceptable.

34. We call the interaction in question major and the others minor. The effect of the mixing of the major interaction with the minor ones should be considered to better understand the dynamic nature of these interactions.

35. The AIM2000 program (Version 2.0) is employed to analyze and visualize atoms-in-molecules: Biegler-König, F. *J. Comput. Chem.* **2000**, *21*, 1040–1048. https://doi.org/10.1002/1096-987x(200009)21:12%3C1040::aid-jcc2%3E3.0.co;2-8

36. Keith, T. A. AIMAll (Version 17.11.14), TK Gristmill Software, Overland Park KS, USA. 2017. Available online: http://aim.tkgristmill.com (accessed on 1st September 2022).

37. θ_p and κ_p for the major bonds/interactions seem to be affected by the behavior of the bonds/interactions around those in question (minor bonds/interactions). Typically, the influence of the behavior of the minor bonds/interactions would not be so severe.

38. Hayashi, S.; Nakanishi, W. *J. Mol. Struct.: THEOCHEM*, **2007**, *811*, 293–301. https://doi.org/10.1016/j.theochem.2007.02.047

39. Hayashi, S.; Nakanishi, W.; Furuta, A.; Drabowicz, J.; Sasamori, T.; Tokitoh, N. *New J. Chem.* **2009**, *33*, 196–206.
https://doi.org/10.1039/b809763a

40. Glendening, E. D.; Badenhoop, J. K.; Reed, A. E.; Carpenter, J. E.; Bohmann, J. A.; Morales, C. M.; Landis, C. R.; Weinhold, F. NBO Version 6.0. 2013.
https://doi.org/10.1002/jcc.23266